NATIONAL ADVISORY COMMITTEE FOR AERONAUTICS

TECHNICAL NOTE 3699

SOME EFFECTS OF JOINT CONDUCTIVITY ON THE TEMPERATURES AND THERMAL STRESSES IN AERODYNAMICALLY HEATED SKIN-STIFFENER COMBINATIONS

By George E. Griffith and Georgene H. Miltonberger

Langley Aeronautical Laboratory
Langley Field, Va.

Washington
June 1956

NATIONAL ADVISORY COMMITTEE FOR AERONAUTICS

TECHNICAL NOTE 3699

SOME EFFECTS OF JOINT CONDUCTIVITY ON THE TEMPERATURES AND THERMAL STRESSES IN AERODYNAMICALLY HEATED SKIN-STIFFENER COMBINATIONS

By George E. Griffith and Georgene H. Miltonberger

SUMMARY

Temperatures and thermal stresses in typical skin-stiffener combinations of winglike structures subjected to aerodynamic heating have been obtained with the aid of an electronic differential analyzer. Variations were made in an aerodynamic heat-transfer parameter, in a joint conductivity parameter, and in the ratio of skin width to skin thickness. The results, which are presented in nondimensional form, indicate that decreasing the joint conductivity parameter lowers both the interior and the average temperature ratios, increases the peak thermal stress ratios in the skin, and may considerably increase the peak stiffener stress ratios; increasing the aerodynamic heat-transfer parameter decreases the interior and average temperature ratios, increases the peak skin stress ratios somewhat, but greatly increases the peak stiffener stress ratios; and increasing the ratio of skin width to skin thickness produces only moderate decreases in the peak skin stress ratios while moderately increasing the peak stiffener stress ratios.

INTRODUCTION

Transient thermal stresses produced by aerodynamic heating of supersonic aircraft may result in buckling, warping, flutter, loss of stiffness, or other deleterious effects which might seriously penalize the performance of the aircraft. In order for the designer to eliminate or minimize these effects, he must know how the thermal stresses are affected by such factors as flight conditions, materials, and the presence of structural discontinuities such as joints. At present, little information is available concerning the effects of joint conductivity on the thermal stresses; such information is needed for the alleviation of these thermal stresses and their accompanying undesirable effects.

The purpose of the theoretical investigation described herein was to determine the effects of joint conductivity on the temperatures and the

thermal stresses in skin-stiffener combinations of winglike structures for different aerodynamic conditions. The work was carried out in nondimensional form with the aid of an electronic differential analyzer. Geometrical effects were included by varying the ratio of skin width to skin thickness, aerodynamic-heating effects by varying the ratio of the product of the boundary-layer heat-transfer coefficient and the skin thickness to the coefficient of thermal conductivity of the material, and joint-conductance effects by varying the ratio of the product of the joint heat-transfer coefficient and the skin thickness to the coefficient of thermal conductivity of the material.

In the present paper the variations in the parameters just described are discussed in terms of their influence on the maximum, minimum, and average temperatures, on the temperature drop across the joint, and on the maximum stresses in the skin and stiffener. These effects are illustrated by an example and then discussed in detail. Equations are developed in appendixes for calculating the temperatures and stresses in the form of dimensionless ratios, and a discussion of the nondimensional parameters is also included as an appendix.

SYMBOLS

A_n	cross-sectional area of element n
b_s	width of skin
b_w	depth of stiffener
c	specific heat of material
E	modulus of elasticity
f	length of joint
h	boundary-layer heat-transfer coefficient
h_j	joint heat-transfer coefficient
$h_j t_s/k$	joint heat-transfer parameter
ht_s/k	aerodynamic heat-transfer parameter (Biot number)
$h\tau/cwt_s$	time parameter

k	thermal conductivity of material
M	Mach number
t_s	skin thickness
t_w	stiffener thickness
T	temperature
T_{av}	average temperature of skin-stiffener structure
T_{AW}	adiabatic-wall temperature
ΔT_j	temperature drop across joint
T_0	initial temperature
w	specific weight of material
α	coefficient of thermal expansion
σ	stress
$\frac{\sigma}{E\alpha(T_{AW} - T_0)}$	stress ratio
τ	time
ϕ	temperature ratio, $\frac{T - T_0}{T_{AW} - T_0}$

Subscripts:

s	skin
w	stiffener

THEORETICAL INVESTIGATION

Problems Investigated

The present investigation consisted of finding the temperatures and thermal stresses in skin-stiffener combinations which were symmetrical about the stiffener center line (fig. 1) and which were symmetrically heated along both skins. Because of symmetry of both the structure and the heating, only one-half the geometry, as shown in figure 1, need be considered in the analysis. This geometry was considered to be at a uniform initial temperature and was then subjected to a step-function change in aerodynamic-heating conditions.

The structure was assumed to be heated in such a way that the heat-transfer coefficient of the boundary layer and the adiabatic-wall temperature did not change with time and were constant along the skin of the structure considered. Similarly, the thermal conductivity of the joint was assumed to have a constant value. The effects of radiation, both internal and external, and the temperature variation through the skin thickness were neglected. It was assumed that there were no heat losses in the system: the only external transfer of heat occurred between the boundary layer and the skin; internal heat transfer took place by conduction; and the heat transfer across the joint was considered to be dependent upon the joint conductance. Material properties were assumed not to change with temperature. In calculating the thermal stresses, the slight dissymmetry about an axis perpendicular to the skin and passing through the midpoint of the joint was neglected, and all deformations of the structure were assumed to be elastic.

As previously mentioned, the work described herein was carried out in terms of nondimensional parameters associated with the particular type of problem considered in this investigation. Hence, the problems considered can be defined in terms of certain of these nondimensional ratios. Changes in the geometry of the structure were achieved by varying the ratio of the skin width to the skin thickness $\left(b_s/t_s = 20, 40, \text{ or } 60\right)$ while all other geometric ratios were held constant $\left(b_w/t_s = 20,\right.$ $t_w/t_s = 0.50$, and $f/t_s = 3.875$; the ratio $f/t_s = 3.875$ was arbitrarily obtained by letting $t_s = 0.250$, $t_w = 0.125$, and $f = 2.5\left(t_w + t_s\right) + 1/32\Big)$. The boundary-layer aerodynamic heat-transfer coefficient was contained in an aerodynamic heat-transfer parameter ht_s/k, commonly referred to as the Biot number; values of ht_s/k used were 0.02, 0.2, and 2. The heat-transfer coefficient of the joint appears in the parameter $h_j t_s/k$. Problems were solved for arbitrarily chosen values of $h_j t_s/k = 0.03$, 0.15, 0.36, and ∞. The special case of $h_j t_s/k = 0$ (zero joint conductivity)

was solved analytically, as shown in appendix A, without using the electronic differential analyzer.

Thus it can be seen that the problems investigated can be described in terms of a geometric ratio b_s/t_s, an aerodynamic heat-transfer parameter ht_s/k, and a joint conductivity parameter $h_j t_s/k$. Problems were solved for all combinations of the parameters mentioned in the preceding paragraph, except that for $b_s/t_s = 60$ and $ht_s/k = 2$ the only problems solved were for $h_j t_s/k = 0$ and ∞.

Theoretical Solution

Inasmuch as the determination of the thermal stresses was the primary objective of this investigation, and since their determination depends upon the distribution of the temperatures, a prerequisite to finding the stresses is a knowledge of the temperatures. Once the temperatures are known, the thermal stresses can be readily obtained (see, for example, ref. 1); however, the evaluation of the stresses, although straightforward, can be cumbersome - depending upon the problem, the simplifying assumptions, and the method of solution.

Solutions to the well-known partial differential equation describing the conductive heat flow in a body are difficult to evaluate by ordinary means for the problem under consideration. Recourse is usually made to a mathematically simpler description of the problem, generally by dividing the structure into a number of elements of finite size (often referred to as lumps). An ordinary differential equation, continuous in time, can then be used to describe the thermal equilibrium of each element, the net result being a system of simultaneous ordinary differential equations equal in number to the number of elements. A closed-form solution for the temperature of any element at any time (provided there are several elements) can only be obtained through a cumbersome and tedious procedure. However, temperature histories for the individual elements can readily be obtained by using either a digital or an analog computer. In this investigation solutions were obtained with the aid of an analog computer known as an electronic differential analyzer. In order to check the solutions for the temperatures a numerical procedure was used to solve sets of finite-difference equations for a few problems wherein the geometry was approximated by using fewer elements and the joint conductivity was considered infinite.

Temperatures.- For a given problem, the cross section of the structure was divided into 15 elements, such as shown in figure 2. (Fig. 2 is a scale drawing of the divided geometry for $b_s/t_s = 40$.) The elements varied in size so that more elements could be concentrated in the region

of the joint and so that, at the same time, the number of elements could be kept to a reasonable minimum. An ordinary differential equation was used to describe the thermal equilibrium of each element, the net result being a system of 15 simultaneous ordinary differential equations. The development of these equations is given in appendix B, and the final set of these equations, written in nondimensional form, is shown in matrix notation at the end of this appendix. The following differential equation for element 5 is presented because it contains all the types of terms found in the complete set of equations. In nondimensional terms, the heat balance for element 5 is given by

$$\frac{d}{d\theta}\left(\frac{T_5 - T_0}{T_{AW} - T_0}\right) + \frac{C_{11}}{\beta}\left(\frac{T_4 - T_0}{T_{AW} - T_0}\right) + \left(1 + \frac{C_{12}}{\beta} + \frac{\beta^{-1}}{\frac{k}{h_j t_s} + \frac{1}{2} + \frac{t_w}{2t_s}}\right)\left(\frac{T_5 - T_0}{T_{AW} - T_0}\right) + \frac{C_{13}}{\beta}\left(\frac{T_6 - T_0}{T_{AW} - T_0}\right) - \frac{\beta^{-1}}{\frac{k}{h_j t_s} + \frac{1}{2} + \frac{t_w}{2t_s}}\left(\frac{T_{11} - T_0}{T_{AW} - T_0}\right) = 1$$

where

$$\theta = h\tau/cwt_s$$

$$\beta = ht_s/k$$

and C_{11}, C_{12}, and C_{13} are dimensionless geometric ratios similar to those shown for equation (B3) in appendix B; the subscripts used are the same as those in appendix B. The temperature ratio for any element is simply the ratio of the temperature rise of the element above the initial temperature to the maximum possible temperature rise.

Thermal stresses.- The assumptions previously mentioned, that material properties do not change with temperature and that the deformations of the structure are elastic, greatly reduce the labor of computation for finding the thermal stresses. If, in addition, there is no thrust or resultant bending moment acting on the cross section (as assumed in the present case), the stress at a point then is directly

proportional to the difference in the average temperature of the structure and the temperature at that point. At any point i, the nondimensional stress ratio (which is treated more fully in appendix C) is given by

$$\frac{\sigma_i}{E\alpha(T_{AW} - T_0)} = -\frac{T_i - T_0}{T_{AW} - T_0} + \frac{T_{av} - T_0}{T_{AW} - T_0}$$

where the stress at a point is given as a fraction of a fictitious or reference thermal stress associated with the maximum possible temperature rise. Hence, the stress ratio can be either positive or negative (indicating tension or compression, respectively) but will always have an absolute value less than 1.

Electronic differential analyzer.- The system of equations for the temperature ratios (appendix B) and the corresponding stress-ratio equations were solved simultaneously by an electronic differential analyzer. A characteristic of this device is that variations in parameters exceeding a range of about 100:1 frequently require reprograming, and, for this reason, cases for which $ht_s/k = 0.002$ were not solved although these cases were included in the original program. Results are obtained from the analyzer by plotting the answers as functions of time or the answers may be read directly from voltmeters at discrete times. The various features of this and other types of high-speed computers or analog methods are discussed in several publications, as, for example, in references 2 to 5.

RESULTS AND DISCUSSION

Data Obtained

Three nondimensional temperature ratios $(T - T_0)/(T_{AW} - T_0)$ and eight nondimensional stress ratios $\sigma/E\alpha(T_{AW} - T_0)$ were plotted against the time parameter $h\tau/cwt_s$ for each problem solved by the electronic differential analyzer. Temperature ratios were obtained for the maximum temperature (element 1), the minimum temperature (element 15), and the average temperature, and stress ratios were obtained for elements 1, 4, 6, 7, 10, 12, 13, and 15. The time scale for both temperature and stress ratios varied from problem to problem. After the analog computer had solved a problem, the stress ratios were examined to find the approximate value of the time parameter at which the maximum stiffener stress ratio had reached its peak value; the problem was then rerun so that voltmeter readings corresponding to all temperature ratios could, if possible, be obtained

shortly before, at, and shortly after the peak stiffener stress ratio. These readings provided the only complete temperature distributions obtained and also aided in establishing values of the time parameter for peak stress ratios and maximum temperature-ratio drops across the joint.

The overall accuracy of the results presented was affected by several sources of error, the magnitudes of which were difficult to determine precisely. However, the maximum error in the temperature ratios was estimated to be less than ± 0.02, and in the stress ratios to be less than ± 0.05. The probable errors should be somewhat lower.

Illustrative Example

In order to illustrate the type of results obtained from the present investigation, the results for a single illustrative problem will be discussed before examining the overall findings. The results for the illustrative problem will be interpreted in terms of a specific material, geometry, and aerodynamic boundary condition. However, the general results of the succeeding sections will be discussed in terms of nondimensional parameters.

Consider, for illustrative purposes, an aircraft wing made of type 302 stainless steel and flying at an altitude of 25,000 feet at a Mach number of 0.9. After reaching an equilibrium temperature of 33° F (corresponding to the adiabatic-wall temperature), the aircraft is suddenly accelerated to a Mach number of 3.0 and then maintains this speed. (See fig. 3(a).) The approximate aerodynamic conditions in this second stage of flight correspond to the following:

$$T_0 = 33^\circ \text{ F}$$

$$M = 3.0$$

$$\text{Altitude} = 25{,}000 \text{ ft}$$

$$h = 0.025 \text{ Btu}/(\text{sq ft})(\text{sec})(^\circ\text{F})$$

$$T_{AW} = 662^\circ \text{ F}$$

The portion of the structure to be analyzed consists of one-half of a skin and stiffener combination which is symmetrical about the stiffener center line and is similar to that shown in figure 1. Thus, with the aid

of figure 1, the geometry can be completely defined with the following quantities:

$$t_s = 0.250 \text{ in.}$$

$$b_s = 10.000 \text{ in.}$$

$$b_w = 5.000 \text{ in.}$$

$$t_w = 0.125 \text{ in.}$$

$$f = 0.969 \text{ in.}$$

The material properties for type 302 stainless steel were taken as (see ref. 6):

$$c = 0.12 \text{ Btu}/(\text{lb})(^\circ\text{F})$$

$$w = 0.29 \text{ lb}/\text{cu in.}$$

$$k = 0.0026 \text{ Btu}/(\text{ft})(\text{sec})(^\circ\text{F})$$

$$E = 28.0 \times 10^6 \text{ lb}/\text{sq in.}$$

$$\alpha = 9.6 \times 10^{-6} \text{ in.}/(\text{in.})(^\circ\text{F})$$

The value of the joint conductivity used for this example is

$$h_j = 67.4 \text{ Btu}/(\text{sq ft})(\text{hr})(^\circ\text{F})$$

$$= 0.0187 \text{ Btu}/(\text{sq ft})(\text{sec})(^\circ\text{F})$$

This value of h_j is lower than expected in the usual stainless-steel joint (see, for example, ref. 7) and corresponds to one in which some type of insulation was used.

The conditions outlined correspond to the problem for which

$$ht_s/k = 0.20$$

$$h_j t_s/k = 0.15$$

$$b_s/t_s = 40$$

The results of the analog computation for the illustrative problem are shown in figures 3 and 4. Figure 3 shows the change with time in the maximum skin temperature (element 1), the minimum temperature in the stiffener (element 15), the average temperature, and the corresponding stresses for elements 1 and 15. The stresses shown are the maximum, in absolute value, for either the skin or the stiffener. Whereas, as seen in figure 3(b), the skin temperature rises rapidly and approximates the maximum possible temperature T_{AW} in about 4 minutes, the stiffener temperature for element 15 lags considerably and requires a considerably longer time to approach T_{AW}. The average temperature of the cross section is much closer to the maximum skin temperature than to the minimum stiffener temperature.

The difference between the average temperature and the skin or stiffener temperature is indicative of the magnitude of thermal stress experienced by element 1 or 15. The difference between the average and the stiffener temperatures is considerably greater than the difference between the average and the skin temperatures; this is reflected in the stress plots in figure 3(c). Since the temperature differences also have different signs, the stresses are of different character, the skin being in compression and the stiffener in tension, as expected. The peak values of the stresses occur at about 2 minutes and 3 minutes for the skin and stiffener, respectively. These times are only a small fraction of the time required for the entire structure to approach the equilibrium temperature but are fairly close to the time required for the skin temperature to stabilize.

Plotted in figure 4 are the temperature and stress distributions for three different times: 0.4 minute, 1.1 minutes, and 1.9 minutes. For simplicity the temperatures and stresses in the skin to the right of the joint have been omitted; the results, if plotted, would be very similar to those shown for the skin to the left of the joint (represented by the symbols and solid lines between points A and B). Up to 1.9 minutes, the skin temperatures have risen sharply, whereas the temperatures of elements 14 and 15 in the stiffener have changed very little. The temperature drop across the joint has increased slightly from 0.4 minute to 1.1 minutes, but there is a slight decrease from 1.1 minutes to 1.9 minutes; this indicates that the time of maximum temperature drop across the joint may be close to 1.1 minutes. (An independent but approximate check of the results gave a time of 1.1 minutes for the maximum temperature drop across the joint for this problem.) As can be seen from figure 4, the temperature drop across the joint has a substantial effect on the stiffener-flange stresses. However, there is no apparent connection between the magnitude of the temperature drop across the joint and the magnitudes of the peak values of the maximum stresses in the skin or stiffener (elements 1 and 15, respectively), nor is there any connection with the times at which these peak stresses occur.

The results shown, which encompass several simplifying assumptions (particularly in regard to the stresses, since, for example, the proportional limit has probably been exceeded), indicate that, although the type 302 stainless steel may well withstand the effects of the temperature level, thermal stresses may develop which are so severe that they dictate design changes.

Temperature and Stress Ratios

Three different sets of geometric ratios were used in the present investigation. These ratios were assigned the following values:

$$b_s/t_s = 20,\ 40,\ 60$$

$$b_w/t_s = 20$$

$$t_w/t_s = 0.50$$

$$f/t_s = 3.875$$

Only the ratio of skin width to skin thickness was varied while the ratios of stiffener depth, stiffener thickness, and length of contact flange of the stiffener to the skin thickness were held constant. For the purpose of discussion it is appropriate to consider first the results which were obtained for a single set of geometric ratios; the geometry selected is for $b_s/t_s = 20$. Results are discussed for this geometry for three values of the aerodynamic heat-transfer parameter ht_s/k (0.02, 0.2, and 2) and for five values of the joint conductivity parameter $h_j t_s/k$ (0, 0.03, 0.15, 0.36, and ∞). The results shown for the case of $h_j t_s/k = 0$ were not calculated by the electronic differential analyzer but were calculated as shown in appendix A. For a brief discussion of all the nondimensional ratios or parameters see appendix D.

$ht_s/k = 0.02$.- Figure 5(a) shows the variation in the maximum, minimum, and average temperature ratios $(T - T_0)/(T_{AW} - T_0)$ plotted against the time parameter $h\tau/cwt_s$ for different values of the joint conductivity parameter $h_j t_s/k$. The aerodynamic heat-transfer parameter was kept constant and was the lowest value used in this investigation $(ht_s/k = 0.02)$. The temperature ratios for element 1 of the skin for cases other than

that for which $h_j t_s/k = 0$ fell slightly below the curve for no conduction along the skin $\left(h_j t_s/k = 0\right)$ but otherwise showed no particular trend and lay within the narrow limits of the two solid curves shown. This small lack of consistency probably reflects inherent inaccuracies in the analog computer. The average temperature ratio and particularly the temperature ratio for element 15 decrease in value as $h_j t_s/k$ decreases, especially as $h_j t_s/k$ approaches zero. For this particular set of conditions, the temperature-ratio changes are fairly moderate for values of the joint conductivity parameter between 0.03 and ∞; however, far greater decreases in the average temperature ratio and the temperature ratio of element 15 of the stiffener occur between joint-conductivity-parameter values of 0.03 and 0. For some materials a value lower than $h_j t_s/k = 0.03$ can probably be obtained only by designing the joint to prevent the flow of heat across it. For example, for $h_j t_s/k = 0.03$ and a value of $h_j = 100$ Btu/(sq ft)(hr)($^\circ$F), the following skin thicknesses would be required for the materials listed: titanium and Inconel X, 0.030 inch; type 302 stainless steel, 0.034 inch; SAE 1020 steel, 0.143 inch; FS1 magnesium, 0.194 inch; and 7075-T aluminum alloy, 0.250 inch. For some of these materials, then, the more moderate changes which occur between joint-conductance ratios of ∞ and 0.03 are indicative of what may be expected for uninsulated joints.

Shown in figure 5(b) are the stress ratios corresponding to the temperature ratios for elements 1 and 15, the maximum values for the skin and for the stiffener. Appreciable increases in the peak values of the stress ratios for both the skin and the stiffener occur as the joint conductivity parameter decreases to zero, but for values of $h_j t_s/k$ between ∞ and 0.03 the increases are more moderate. The positive and negative signs of the stress ratios indicate, as expected, that the cool stiffener is in tension while the hot skin is in compression. It can be noted that values of the peak stress ratios, for either the skin or stiffener, occur at values of the time parameter which increase with decreasing values of the joint conductivity parameter and, also, that peak values for the skin and stiffener for a particular set of conditions do not occur at the same value of the time parameter.

$ht_s/k = 0.2$.- Figure 6(a) shows the effect on the temperature ratios (maximum, minimum, and average) of varying the joint conductivity parameter for the same geometry $\left(b_s/t_s = 20\right)$ and an aerodynamic heat-transfer parameter of 0.2. The results show that there is an insignificant change produced in the maximum temperature ratio (element 1 in the skin), a noticeable lowering of the average temperature ratio when the joint conductivity parameter decreases in value, and a similar but more pronounced change in the minimum temperature ratio (element 15 in the stiffener).

Figure 6(b) shows the corresponding effect on the stress ratios. The peak values of the maximum skin stress ratio (element 1) increase as the joint conductivity parameter decreases; this is due to the fact that while the skin temperature ratio did not change appreciably, the average temperature ratio decreased somewhat as the joint conductivity parameter decreased, thereby causing a corresponding increase in the difference in the temperature ratios (upon which the size of the stress ratio depends). The peak values of the stiffener stress ratios (element 15) are much larger than for the skin and tend to decrease very slightly with decreasing values of the joint conductivity parameter. Thus, for this particular combination of configuration and aerodynamic heat-transfer parameter, there is very little change produced in the peak stiffener stress ratio by varying the value of the joint conductivity parameter. However, the results indicate, as might be expected, that the case of zero joint conductivity does not provide an upper limit to the peak stiffener stress ratio.

$ht_s/k = 2$.- Similar results for both the temperature and stress ratios for the same geometry $\left(b_s/t_s = 20\right)$ and an aerodynamic heat-transfer parameter of 2 are shown in figure 7. This value of ht_s/k corresponds to rather severe heating rates. Figure 7(a) shows that increasing $h_j t_s/k$ from 0 to ∞ produces no discernible change in the temperature ratios for elements 1 and 15 and only a moderate increase in the average temperature ratio. Hence, for this high value of ht_s/k the effect of the joint conductivity parameter is relatively unimportant, since, as expected, the skin temperature ratio approaches its limiting value before heat can be conducted into the interior, regardless of the conductivity of the joint. This results, as seen in figure 7(b), in only moderate change in either of the stress ratios. The peak skin stress ratio increases as the joint conductivity parameter decreases. However, it can be noted that the peak stiffener stress ratio again decreases with decreasing $h_j t_s/k$; this is expected since the average temperature ratio decreases while the stiffener temperature ratio stays close to zero, so that the differences in the temperature ratios also decrease. Thus, it can again be seen that, at the larger values of ht_s/k, the case of $h_j t_s/k = 0$ does not constitute an upper limit to the maximum stiffener stress ratio.

$b_s/t_s = 20$.- The results discussed so far are grouped in figure 8 so that, for this particular geometry $\left(b_s/t_s = 20\right)$, the influences of the aerodynamic heat-transfer parameter and the joint conductivity parameter can be seen simultaneously. Curves are included for values of $h_j t_s/k = 0$, 0.03, and ∞, so that both the change occurring between $h_j t_s/k = 0$ and 0.03 and the change between $h_j t_s/k = 0.03$ and ∞ can be observed. When the range of $h_j t_s/k$ from 0 to 0.03 is excluded, the

results indicate that the aerodynamic heat-transfer parameter may produce more change in both the temperature and peak stress ratios than is produced by changing the joint conductivity ratio from 0.03 to ∞. (This, however, includes an exceptionally wide range in ht_s/k.) In general, even greater changes occur as $h_j t_s/k$ diminishes from 0.03 to 0.

b_s/t_s = 40 and 60.- Plotted in figures 9 and 10 are composite results similar to those of figure 8 but for values of the geometric ratio b_s/t_s = 40 and 60, respectively. Figure 10 shows no temperature- or stress-ratio curve for $h_j t_s/k = 0.03$ and $ht_s/k = 2$, since, for this geometry and $ht_s/k = 2$, the only case solved by the electronic differential analyzer was for $h_j t_s/k = \infty$. However, it is apparent from an inspection of figure 10 that, as previously mentioned (see the section for $ht_s/k = 2$), the effect of varying $h_j t_s/k$ is small when $ht_s/k = 2$, especially so for $b_s/t_s = 60$. The results presented in figures 9(a) and 10(a) show that the temperature ratios behave as expected; there is little or no change in the temperature ratio for element 1, but both the average temperature ratio and that for element 15 decrease with increasing ht_s/k and with decreasing $h_j t_s/k$. Note that for figures 8(a), 9(a), and 10(a) the curves for element 15 for $ht_s/k = 2$ and for any case where $h_j t_s/k = 0$ lie close to or along the zero axis.

The peak values of the skin stress ratio for element 1 increase with increasing ht_s/k and with decreasing $h_j t_s/k$. (See figs. 9(b) and 10(b).) For element 15 the peak stiffener stress ratios also increase with increasing ht_s/k. However, these stiffener stress ratios may either increase or decrease with decreasing $h_j t_s/k$; this is so because when ht_s/k is small the difference in the average temperature ratio and that for element 15 always increases as $h_j t_s/k$ decreases, whereas as ht_s/k gets larger the difference in these temperature ratios begins to decrease with decreasing $h_j t_s/k$. The results shown in figures 8(b), 9(b), and 10(b) again illustrate that, although the case of zero joint conductivity constitutes an upper limit to the peak skin stress ratio, the upper limit to the peak stiffener stress ratio is not that for $h_j t_s/k = 0$.

Effect of geometric ratio b_s/t_s.- Although the overall effects of changing b_s/t_s - the only geometric change effected - can be seen by studying figures 5 to 10, some of these results have been replotted in figures 11, 12, and 13 in order that they may be more readily studied. These latter figures show the temperature and stress ratios for $ht_s/k = 0.2$, for values of $h_j t_s/k = 0$, 0.03, and ∞, respectively, and for values of $b_s/t_s = 20$, 40, and 60.

Figure 11 shows results for the case of zero joint conductivity ($h_j t_s/k = 0$) which were obtained as outlined in appendix A (and not by using the electronic differential analyzer). The only change in the temperature ratios occurs in the average temperature ratio, which increases as b_s/t_s increases. Figure 11 also shows that the stiffener stress ratios increase and that the skin stress ratios decrease as b_s/t_s increases, with the major changes occurring between $b_s/t_s = 20$ and 40. The values of the time parameter at which the peak values of these stress ratios occur are theoretically infinite, but, for practical purposes, can be seen to have been reached at values of $h\tau/cwt_s$ of about 6 and 4 for the stiffener and skin, respectively. In general, the major result of increasing the ratio b_s/t_s is effectively to put a greater proportion of the mass in the skin, thereby raising the average temperature ratio while having little or no effect on the magnitudes of the temperature ratios for elements 1 and 15. Thus, the difference between the skin temperature ratio and the average temperature ratio will decrease as b_s/t_s is increased, and the corresponding thermal-stress ratio for element 1 will likewise decrease. On the other hand, the difference in the stiffener temperature ratio for element 15 and the average temperature ratio will increase with increasing b_s/t_s, so that the corresponding stress ratio for element 15 will also increase.

Figure 12 shows results for $ht_s/k = 0.2$ and $h_j t_s/k = 0.03$. Again, as expected, there is little change in the temperature ratios for elements 1 and 15, but a progressive increase occurs in the value of the average temperature ratio as b_s/t_s is increased, with more change occurring between $b_s/t_s = 20$ and 40 than between 40 and 60. The stress-ratio results are similar to those shown in figure 11(b) for $h_j t_s/k = 0$ and, again, there is a slightly larger increase in the stiffener stress ratio and a correspondingly larger decrease in the skin stress ratio between $b_s/t_s = 20$ and 40 than between 40 and 60. The value of the time parameter for which peak values of the stiffener stress ratios occur decreases as b_s/t_s increases, whereas there is apparently little change in the time parameter for peak values of the skin stress ratios.

The results shown in figure 13 for $ht_s/k = 0.2$ and $h_j t_s/k = \infty$ have essentially the same characteristics as those just discussed for $ht_s/k = 0.2$ and $h_j t_s/k = 0.03$ and shown in figure 12. The collective results shown in figures 11, 12, and 13 illustrate that, for a point approximately 10 times the skin thickness or greater away from a heat sink, conduction toward the heat sink will make little or no difference in the temperature rise at that point. The effects of heat conduction near the heat sink will be more noticeable for low values of ht_s/k and for high values of $h_j t_s/k$.

The results shown in figures 11, 12, and 13 illustrate the effects of changing b_s/t_s for $ht_s/k = 0.2$ and are typical of the results in general. A more complete study of the effects of changing b_s/t_s can be made by examining the results shown in figures 5 to 10.

Peak Stress Ratios and Temperature-Ratio Drop Across Joint

Variation of skin stress ratio (element 1) with $h_j t_s/k$.- The peak values of the stress ratios for element 1 of the skin are plotted against $h_j t_s/k$ in figure 14(a). This plot shows that there is a separate curve for each combination of ht_s/k and b_s/t_s. (There is no curve for $ht_s/k = 2$ and $b_s/t_s = 60$, since, of this group, the only problem solved was that for which $h_j t_s/k = \infty$.) The results show that the peak skin stress ratio decreases as b_s/t_s increases, which indicates that, as the proportion of skin area to total cross-sectional area increases, the average temperature ratio gets closer to the skin temperature ratio. The stress ratios do not change much as $h_j t_s/k$ decreases, except that as $h_j t_s/k$ approaches zero the peak skin stress ratio may increase appreciably, especially for low values of ht_s/k.

The values of the time parameter which correspond to the peak skin stress ratios are plotted in figure 14(b) against $h_j t_s/k$. The results show that the value of the time parameter is essentially independent of the geometry and hence that a single curve can be drawn for each value of ht_s/k. The time parameter increases with increasing ht_s/k and also increases with decreasing $h_j t_s/k$, especially as $h_j t_s/k$ approaches zero.

Variation of stiffener stress ratio (element 15) with $h_j t_s/k$.- Peak stiffener stress ratios are plotted against $h_j t_s/k$ in figure 15(a). Again, there is no curve for $ht_s/k = 2$ and $b_s/t_s = 60$. In some cases for which $ht_s/k = 2$, the stiffener stress ratio may not have reached its absolute peak value, since these stress ratios were leveling off as the computer was stopped. (See, for example, figs. 8 and 9.) For this reason the peak values shown in figure 15(a) are less reliable (only, it is believed, by a small amount) for these cases than for the others. As shown for the skin, there is a separate curve for each combination of ht_s/k and b_s/t_s. The plotted results indicate that the peak stiffener stress ratio increases as ht_s/k increases from 0.02 to 0.2, and again increases, but

not nearly so much, as ht_s/k increases from 0.2 to 2. The magnitudes of these changes depend upon $h_j t_s/k$; below a value of $h_j t_s/k$ of about 0.15, these changes diminish to zero (at $h_j t_s/k = 0$); above $h_j t_s/k = 0.15$, the change with ht_s/k is essentially constant. The results also show that as $h_j t_s/k$ approaches zero the peak stress ratio may either increase appreciably at low values of ht_s/k or decrease slightly at high values of ht_s/k.

Values of the time parameter corresponding to the peak stiffener stress ratios are plotted against $h_j t_s/k$ in figure 15(b). Since, as explained in the preceding paragraph, there was some difficulty in a precise determination of the peak stiffener stress ratio for some cases for which $ht_s/k = 2$, it was impossible to determine the corresponding values of the time parameter, and hence no data are presented for these cases. Within the limits of accuracy of the analog computer, the results shown appear to be essentially independent of b_s/t_s. These limited results indicate that the time parameter increases appreciably as ht_s/k increases from 0.02 to 0.2. The results also reveal that the time parameter increases very slightly as $h_j t_s/k$ decreases, except at the very low values of $h_j t_s/k$ where the increase is more pronounced.

Variation of temperature-ratio drop across joint with $h_j t_s/k$.- The effects of varying the joint conductivity parameter $h_j t_s/k$ on the temperature and stress ratios for elements 1 and 15 have been discussed in the preceding sections. Also of some interest is the effect on the temperature-ratio drop across the joint. Shown in figure 16, plotted against $h_j t_s/k$, are the maximum values of the temperature-ratio drop across the joint (that is, from element 6 to element 12) and the values of the time parameter at which these maximum drops occur. The results shown for the temperature-ratio drop and the time parameter are similar. Varying the geometric ratio b_s/t_s from 20 to 60 seems to have little or no effect, as expected; hence, a single curve can be drawn through the points for each value of ht_s/k. Both the maximum temperature-ratio drop and the corresponding value of the time parameter are affected by ht_s/k and $h_j t_s/k$; both decrease in value as ht_s/k decreases and as $h_j t_s/k$ increases. This result is expected, since either decreasing ht_s/k or increasing $h_j t_s/k$ tends to permit freer conduction of heat in the structure.

Neither the maximum temperature-ratio drops across the joint nor the corresponding values of the time parameter have been correlated with the peak skin or stiffener stress ratios and their associated time parameters.

It is believed that so many factors affect the temperature- and stress-ratio distributions and the magnitudes of the peak stresses that no such correlation can readily be made. Essentially, the same peak stresses may be produced in many ways. For illustrative purposes, figure 17 shows three temperature- and stress-ratio distributions. (These results were taken from three different problems at values of the time parameter slightly less than that required for peak stiffener stress ratios.) Although rather insignificant changes have occurred in the peak stiffener stress ratio (point D of element 15) and not much change in the peak skin stress ratio (point A of element 1), the joint conductivity parameter can be seen to have had a tremendous effect on both the temperature and stress ratios in the vicinity of the joint.

CONCLUDING REMARKS

A theoretical investigation was conducted to determine the influence of joint conductivity on the temperatures and thermal stresses in aerodynamically heated skin-stiffener combinations of winglike structures. Varying the ratio of skin width to skin thickness, the aerodynamic heat-transfer parameter, and the joint conductivity parameter indicated the following results.

Increasing the ratio of skin width to skin thickness raised the average temperature ratio without notably changing the other temperature ratios, moderately decreased the peak skin stress ratios while moderately increasing the peak stiffener stress ratios, and had no apparent influence on the values of the time parameters associated with the peak stress ratios.

Increasing the aerodynamic heat-transfer parameter produced the following results: considerably altered the distribution of the temperature ratios by increasing the temperature-ratio drop across the joint, lowering the minimum temperature ratio in the stiffener, and also lowering, but to a considerably lesser extent, the average temperature ratio; appreciably increased the peak stiffener stress ratios while only moderately increasing the peak skin stress ratios; and increased the values of the time parameter for both the peak stress ratios.

Decreasing the joint conductivity parameter produced the following results: increased the temperature-ratio drop across the joint and lowered the average temperature ratio and the minimum stiffener temperature ratio; increased the peak skin stress ratios appreciably only at low values of both the joint conductivity parameter and the Biot number; increased the peak stiffener stress ratio appreciably at the low values of the heat-transfer parameter but decreased the peak stiffener stress ratios slightly at the high values of the heat-transfer parameter; and had little

effect on the time parameter associated with the peak stresses, except to increase the time parameter sharply as the joint conductivity parameter approached zero.

Langley Aeronautical Laboratory,
National Advisory Committee for Aeronautics,
Langley Field, Va., March 14, 1956.

APPENDIX A

SPECIAL CASE OF ZERO JOINT CONDUCTIVITY

Temperatures

For the case of zero joint conductivity, the temperature rise anywhere in the skin is given by the well-known differential equation (normally used when conduction effects are ignored)

$$cwt_s \frac{dT_s}{d\tau} = h(T_{AW} - T_s) \tag{A1}$$

The solution to equation (A1) can be written in terms of the nondimensional temperature rise of the skin (provided that, as previously assumed, c, w, and h are constant with time)

$$\frac{T_s - T_0}{T_{AW} - T_0} = 1 - e^{-\frac{h\tau}{cwt_s}} \tag{A2}$$

Since no heat can be conducted across the joint, the entire stiffener remains at the initial temperature; hence, the nondimensional temperature ratio for the stiffener is zero. Thus, the average nondimensional temperature of the structure is given by

$$\frac{T_{av} - T_0}{T_{AW} - T_0} = \frac{t_s b_s}{\sum_{n=1}^{15} A_n}\left(1 - e^{-\frac{h\tau}{cwt_s}}\right) \tag{A3}$$

where A_n is the cross-sectional area of element n.

Stresses

The thermal stress at any point in a structure depends upon the difference in the temperature at the point and the average temperature (see, for example, refs. 1 and 8); hence, for the skin the nondimensional stress ratio is

$$\frac{\sigma_s}{E\alpha(T_{AW} - T_0)} = -\frac{T_s - T_0}{T_{AW} - T_0} + \frac{T_{av} - T_0}{T_{AW} - T_0}$$

$$= \left(\frac{t_s b_s}{\sum_{n=1}^{15} A_n} - 1\right)\left(1 - e^{-\frac{h\tau}{cwt_s}}\right) \tag{A4}$$

and for the stiffener

$$\frac{\sigma_w}{E\alpha(T_{AW} - T_0)} = \frac{t_s b_s}{\sum_{n=1}^{15} A_n}\left(1 - e^{-\frac{h\tau}{cwt_s}}\right) \tag{A5}$$

APPENDIX B

DIFFERENTIAL EQUATIONS FOR CALCULATING TEMPERATURES

Equations of heat balance are derived for three typical elements in a skin and stiffener combination such as shown in figure 2. The assumptions made in this analysis regarding the temperatures are as follows:

(1) The heat-transfer coefficient of the boundary layer is constant along the skin at any time.

(2) The temperature is uniform throughout any element but for analytical purposes is considered concentrated at the center of the element; end elements 1, 10, and 15 are considered to be one-half of symmetrical elements.

(3) Each element receives heat directly only from adjacent elements and, if a skin element, from the boundary layer.

(4) Radiation effects can be neglected.

(5) Material properties do not change with temperature.

(6) Joint conductivity does not change with temperature.

(7) The skin and stiffener are made of the same material.

Typical Skin Element

Consider first a typical skin element (other than element 5 or 6), such as element 3, with the quantities of heat which influence its temperature (per unit depth, where the depth direction is perpendicular to the cross section of the structure) shown by the following sketch:

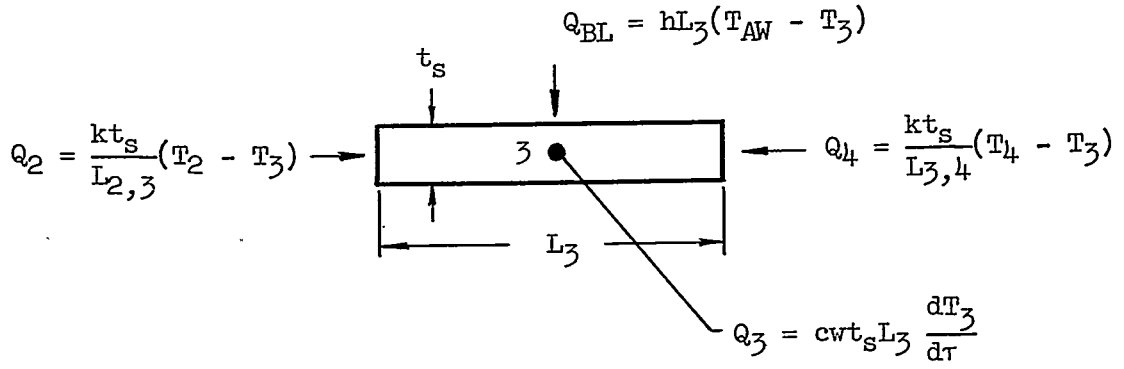

where

Q rate of heat flow or heat stored

$L_{2,3}$ distance between centers of elements 2 and 3

$L_{3,4}$ distance between centers of elements 3 and 4

Thermal equilibrium requires that the rate of heat stored Q_3 be equal to the sum of the rates of heat entering and leaving, $Q_{BL} + Q_2 + Q_4$, so that

$$cwt_s L_3 \frac{dT_3}{d\tau} = hL_3(T_{AW} - T_3) + \frac{kt_s}{L_{2,3}}(T_2 - T_3) + \frac{kt_s}{L_{3,4}}(T_4 - T_3) \qquad (B1)$$

Subtracting T_0 from each temperature, dividing through by $hL_3(T_{AW} - T_0)$, and converting to nondimensional time $\left(\text{where } \theta = \frac{h\tau}{cwt_s}\right)$ gives equation (B1) in nondimensional form

$$\frac{d}{d\theta}\left(\frac{T_3 - T_0}{T_{AW} - T_0}\right) - \frac{kt_s}{hL_3L_{2,3}}\left(\frac{T_2 - T_0}{T_{AW} - T_0}\right) + \left(1 + \frac{kt_s}{hL_3L_{2,3}} + \frac{kt_s}{hL_3L_{3,4}}\right)\left(\frac{T_3 - T_0}{T_{AW} - T_0}\right) - \frac{kt_s}{hL_3L_{3,4}}\left(\frac{T_4 - T_0}{T_{AW} - T_0}\right) = 1 \qquad (B2)$$

which can be simplified to

$$\ddot{\phi}_3 + \frac{C_5}{\beta}\phi_2 + \left(1 + \frac{C_6}{\beta}\right)\phi_3 + \frac{C_7}{\beta}\phi_4 = 1 \qquad (B3)$$

where

$$\ddot{\phi}_3 = \frac{d}{d\theta}\left(\frac{T_3 - T_0}{T_{AW} - T_0}\right)$$

$$\beta = \frac{ht_s}{k}$$

and C_5, C_6, and C_7 are dimensionless geometric ratios which are the same as those appearing at the end of this appendix where the equations for all the elements are given in matrix form.

Note that although the h used herein pertaining to the skin is described as the boundary-layer heat-transfer coefficient, this coefficient could, in substance, be an effective heat-transfer coefficient, a combination of the heat-transfer coefficient of the boundary layer and the thermal conductivity of some surface insulator divided by its thickness t. This effective heat-transfer coefficient, which would then replace h in the calculations, would be related to the latter by the equation

$$\frac{1}{h_{effective}} = \frac{1}{h} + \left(\frac{t}{k}\right)_{insulator}$$

Using $h_{effective}$ would give accurate results, provided little heat is stored in the insulator. Thus, the results reported may be interpreted for either insulated or uninsulated skins.

Element Affected by Joint

Before deriving similar equations for the elements affected by the joint, it is desirable to develop an expression for the heat transfer between elements separated by the joint such that this expression contains both the heat-transfer coefficient of the joint and the thermal conductivity of the material. Consider, for example, elements 5 and 11 which are separated by a joint of negligible thickness but of finite conductivity such that a drop in temperature takes place across the joint, as shown in the following sketch:

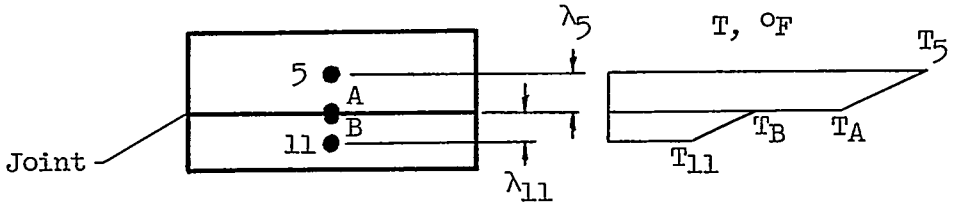

Across the joint, since there is no storage of heat,

$$\frac{k}{\lambda_5}(T_5 - T_A) = h_j(T_A - T_B) = \frac{k}{\lambda_{11}}(T_B - T_{11}) \qquad (B4)$$

Solving equations (B4) for T_A and T_B in terms of T_5 and T_{11} gives

$$T_A = \frac{\left(\frac{h_j}{\lambda_5} + \frac{k}{\lambda_5\lambda_{11}}\right)T_5 + \frac{h_j}{\lambda_{11}} T_{11}}{\frac{h_j}{\lambda_5} + \frac{h_j}{\lambda_{11}} + \frac{k}{\lambda_5\lambda_{11}}} \tag{B5}$$

and

$$T_B = \frac{\frac{h_j}{\lambda_5} T_5 + \left(\frac{h_j}{\lambda_{11}} + \frac{k}{\lambda_5\lambda_{11}}\right)T_{11}}{\frac{h_j}{\lambda_5} + \frac{h_j}{\lambda_{11}} + \frac{k}{\lambda_5\lambda_{11}}} \tag{B6}$$

But, since there is no loss or storage of heat,

$$h_j(T_A - T_B) = h'(T_5 - T_{11}) \tag{B7}$$

where h' is a coefficient which contains both the thermal conductivity of the material, divided by appropriate distances, and the heat-transfer coefficient of the joint. Solving equation (B7) for h' by substituting T_A and T_B from equations (B5) and (B6), respectively, gives

$$h' = \frac{1}{\frac{1}{h_j} + \frac{\lambda_5}{k} + \frac{\lambda_{11}}{k}} \tag{B8}$$

Equation (B8) is the expected result and is analogous to the well-known thermal series-resistance equation. (See, for example, ref. 9.)

Since $\lambda_5 = t_s/2$ and $\lambda_{11} = t_w/2$, equation (B8) can be written

$$h' = \frac{2}{\frac{2}{h_j} + \frac{t_s}{k} + \frac{t_w}{k}} = h_j \frac{1}{1 + \frac{h_j t_s}{2k}\left(1 + \frac{t_w}{t_s}\right)} \tag{B9}$$

The value of h' is largely governed by the value of h_j, so that, as might be expected, the terms t_s/k and t_w/k could be omitted with very little loss in accuracy when h_j is small (that is, when its reciprocal is large and h' is therefore small). However, the values of the k terms are more significant and cannot be neglected as h_j increases in value (and its reciprocal decreases).

Now consider element 5 with the quantities of heat which affect its temperature rise, as shown in the following sketch:

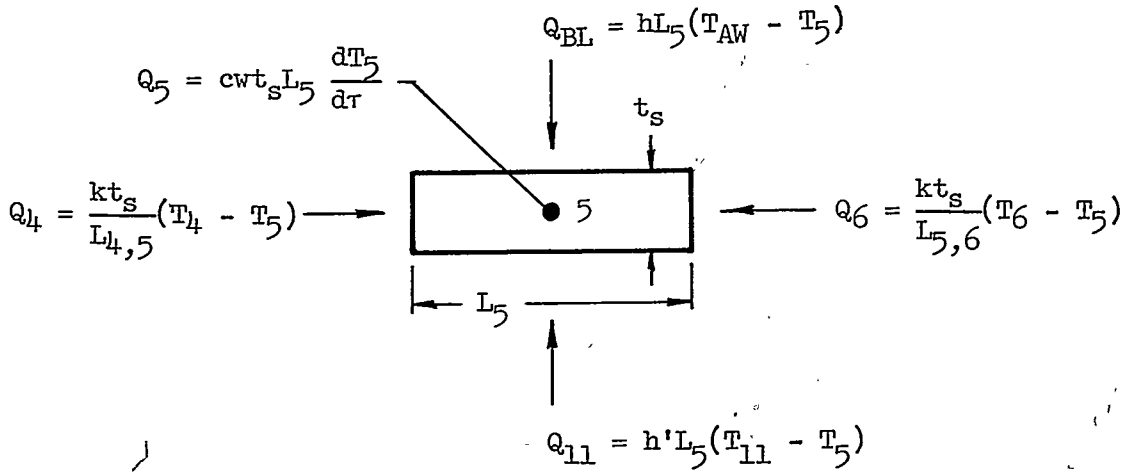

where the notation is similar to that used in obtaining equation (B1). Hence,

$$cwt_sL_5 \frac{dT_5}{d\tau} = hL_5(T_{AW} - T_5) + \frac{kt_s}{L_{4,5}}(T_4 - T_5) + \frac{kt_s}{L_{5,6}}(T_6 - T_5) + h'L_5(T_{11} - T_5) \tag{B10}$$

Proceeding as before, equation (B10) can be written in nondimensional form as

$$\dot{\phi}_5 + \frac{C_{11}}{\beta}\phi_4 + \left(1 + \frac{C_{12}}{\beta} + \frac{\beta^{-1}}{\frac{k}{h_jt_s} + \frac{1}{2} + \frac{t_w}{2t_s}}\right)\phi_5 + \frac{C_{13}}{\beta}\phi_6 - \frac{\beta^{-1}}{\frac{k}{h_jt_s} + \frac{1}{2} + \frac{t_w}{2t_s}}\phi_{11} = 1 \tag{B11}$$

The dimensionless ratios C_{11}, C_{12}, and C_{13} are the same as those used in the text and in the equations at the end of this appendix.

Typical Stiffener Element

For a typical element unaffected by heat from the boundary layer, for example element 14, the quantities of heat which affect its temperature rise are shown in the following sketch:

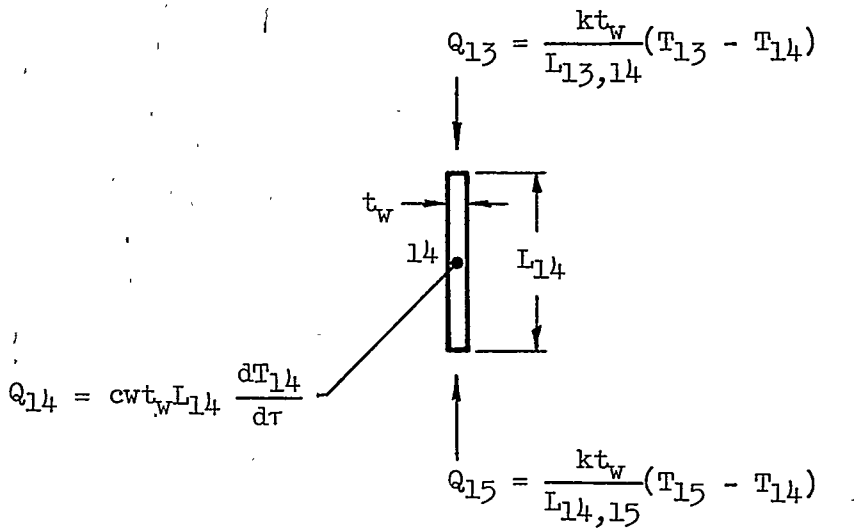

As before,

$$cwt_wL_{14}\frac{dT_{14}}{d\tau} = \frac{kt_w}{L_{13,14}}(T_{13} - T_{14}) + \frac{kt_w}{L_{14,15}}(T_{15} - T_{14}) \qquad (B12)$$

Equation (B12) can be simplified to give

$$\dot{\phi}_{14} + \frac{C_{21}}{\beta}\phi_{13} + \frac{C_{22}}{\beta}\phi_{14} + \frac{C_{23}}{\beta}\phi_{15} = 0 \qquad (B13)$$

Again, the coefficients C_{21}, C_{22}, and C_{23} are the same as those given in the matrix of the complete set of equations. Similarly, equations can be written for the remaining elements.

Nondimensional Equations for Aerodynamically Heated 15-Element Structure

The result of writing the equations for the remaining elements can be conveniently expressed in matrix notation as follows:

$$\left[a_{n,m}\right]\left\{\phi_m\right\} = \left\{p_n\right\}$$

$$a_{1,1} = a_{10,10} = \frac{d}{d\theta} + 1 + \frac{C_1}{\beta}$$

$$a_{1,2} = a_{10,9} = -\frac{C_1}{\beta}$$

$$a_{2,1} = a_{9,10} = \frac{C_2}{\beta}$$

$$a_{2,2} = a_{9,9} = \frac{d}{d\theta} + 1 + \frac{C_3}{\beta}$$

$$a_{2,3} = a_{9,8} = \frac{C_4}{\beta}$$

$$a_{3,2} = a_{8,9} = \frac{C_5}{\beta}$$

$$a_{3,3} = a_{8,8} = \frac{d}{d\theta} + 1 + \frac{C_6}{\beta}$$

$$a_{3,4} = a_{8,7} = \frac{C_7}{\beta}$$

$$a_{4,3} = a_{7,8} = \frac{C_8}{\beta}$$

$$a_{4,4} = a_{7,7} = \frac{d}{d\theta} + 1 + \frac{C_9}{\beta}$$

$$a_{4,5} = a_{7,6} = \frac{C_{10}}{\beta}$$

$$a_{5,4} = a_{6,7} = \frac{C_{11}}{\beta}$$

$$a_{5,5} = a_{6,6} = \frac{d}{d\theta} + 1 + \frac{C_{12}}{\beta} + \Omega$$

$$a_{5,6} = a_{6,5} = \frac{C_{13}}{\beta}$$

$$a_{5,11} = a_{6,12} = a_{11,5} = a_{12,6} = -\Omega$$

$$a_{11,11} = \frac{d}{d\theta} + \frac{C_{14}}{\beta} + \Omega$$

$$a_{11,12} = -\frac{C_{14}}{\beta}$$

$$a_{12,11} = \frac{C_{15}}{\beta}$$

$$a_{12,12} = \frac{d}{d\theta} + \frac{C_{16}}{\beta} + \Omega$$

$$a_{12,13} = \frac{C_{17}}{\beta}$$

$$a_{13,12} = \frac{C_{18}}{\beta}$$

$$a_{13,13} = \frac{d}{d\theta} + \frac{C_{19}}{\beta}$$

$$a_{13,14} = \frac{C_{20}}{\beta}$$

$$a_{14,13} = \frac{C_{21}}{\beta}$$

$$a_{14,14} = \frac{d}{d\theta} + \frac{C_{22}}{\beta}$$

$$a_{14,15} = \frac{C_{23}}{\beta}$$

$$a_{15,14} = -\frac{C_{24}}{\beta}$$

$$a_{15,15} = \frac{d}{d\theta} + \frac{C_{24}}{\beta}$$

All other $a_{n,m} = 0$

where

$$p_1 = p_2 = \cdots = p_{10} = 1$$

$$p_{11} = p_{12} = \cdots = p_{15} = 0$$

$$\beta = ht_s/k$$

$$\theta = h\tau/cwt_s$$

$$\Omega = \frac{\beta^{-1}}{\frac{k}{h_j t_s} + \frac{1}{2} + \frac{t_w}{2t_s}}$$

and

$C_1 = t_s^2/L_1L_{1,2}$

$C_2 = -t_s^2/L_2L_{1,2}$

$C_3 = -C_2 - C_4$

$C_4 = -t_s^2/L_2L_{2,3}$

$C_5 = -t_s^2/L_3L_{2,3}$

$C_6 = -C_5 - C_7$

$C_7 = -t_s^2/L_3L_{3,4}$

$C_8 = -t_s^2/L_4L_{3,4}$

$C_9 = -C_8 - C_{10}$

$C_{10} = -t_s^2/L_4L_{4,5}$

$C_{11} = -t_s^2/L_5L_{4,5}$

$C_{12} = -C_{11} - C_{13}$

$C_{13} = -t_s^2/L_5L_{5,6}$

$C_{14} = t_s^2/L_{11}L_{11,12}$

$C_{15} = -t_s^2/L_{12}L_{11,12}$

$C_{16} = -C_{15} - C_{17}$

$C_{17} = -t_s^2/L_{12}L_{12,13}$

$C_{18} = -t_s^2/L_{13}L_{12,13}$

$C_{19} = -C_{18} - C_{20}$

$C_{20} = -t_s^2/L_{13}L_{13,14}$

$C_{21} = -t_s^2/L_{14}L_{13,14}$

$C_{22} = -C_{21} - C_{23}$

$C_{23} = -t_s^2/L_{14}L_{14,15}$

$C_{24} = t_s^2/L_{15}L_{14,15}$

APPENDIX C

THERMAL-STRESS EQUATIONS

Since the stresses depend upon the temperatures, the assumptions used in calculating the temperatures also apply to the stresses. In addition, the following assumptions were incorporated in calculating the stresses:

(1) The cross section and temperature distribution are constant in the direction perpendicular to the cross section, the cross section under consideration is far enough from the end of the structure to be free of any end effects, and only self-equilibrating thermal stresses act on the cross section.

(2) The section considered is one-half of a section which is symmetrical about the stiffener center line.

(3) The slight dissymmetry about an axis through the joint center line is considered to have a negligible effect and is thus ignored.

(4) The stresses and strains are entirely elastic, and the modulus of elasticity does not change with temperature.

In accord with the aforementioned assumptions and those used in the determination of the temperatures, the stresses may be calculated directly (see refs. 1 and 8) from the equation

$$\sigma_i = E\alpha(-T_i + T_{av})$$

$$= -E\alpha T_i + \frac{E\alpha \sum_{n=1}^{15} T_n A_n}{\sum_{n=1}^{15} A_n} \qquad (C1)$$

where

σ_i stress in element i

T_i temperature of element i

T_{av} average temperature of cross section, $\sum_{n=1}^{15} T_n A_n \Big/ \sum_{n=1}^{15} A_n$

Equation (C1) can be written in terms of a nondimensional stress ratio and nondimensional temperature ratios as

$$\frac{\sigma_i}{E\alpha(T_{AW} - T_0)} = -\frac{T_i - T_0}{T_{AW} - T_0} + \frac{\sum_{n=1}^{15} \frac{T_n - T_0}{T_{AW} - T_0} A_n}{\sum_{n=1}^{15} A_n}$$

$$= -\phi_i + \frac{\sum_{n=1}^{15} \phi_n A_n}{\sum_{n=1}^{15} A_n} \qquad (C2)$$

APPENDIX D

NONDIMENSIONAL RATIOS

The problems solved in this investigation and the results obtained have been described in terms of the natural parameters or nondimensional ratios associated with the particular type of problem investigated. (See appendixes B and C.) The parameters which define a particular problem, once they have been assigned specific values, are b_s/t_s, b_w/t_s, f/t_s, t_w/t_s, ht_s/k, and $h_j t_s/k$. Of these parameters, the first four define the geometry and the last two the boundary conditions. For prescribed values of these six nondimensional ratios (together with initial conditions) there exists a unique set of nondimensional temperature ratios $(T - T_0)/(T_{AW} - T_0)$ and stress ratios $\sigma/E\alpha(T_{AW} - T_0)$ which vary with the time parameter $h\tau/cwt_s$ (also nondimensional).

Physical Significance

The parameters b_s/t_s, b_w/t_s, f/t_s, and t_w/t_s are obvious geometric ratios which give the dimensions of the structure in terms of the skin thickness. The parameter ht_s/k, the Biot number, is the ratio of the surface heat-transfer coefficient to the internal heat-transfer coefficient (the coefficient of thermal conductivity of the material), multiplied by a basic dimension which is characteristic of this problem, the skin thickness. Similarly, the parameter $h_j t_s/k$ is the ratio of the joint heat-transfer coefficient to the internal heat-transfer coefficient, multiplied by the skin thickness. The ratio $(T - T_0)/(T_{AW} - T_0)$ defines the temperature rise (above the initial temperature) at a point as a fraction of the maximum possible temperature rise. The stress ratio $\sigma/E\alpha(T_{AW} - T_0)$ gives the stress at a point in terms of a reference thermal stress associated with the maximum possible temperature rise $(T_{AW} - T_0)$. The time parameter $h\tau/cwt_s$ is the ratio of the surface heat-transfer coefficient to the heat absorptive capacity of the skin, multiplied by the time, or the time parameter may also be considered as the ratio of the actual time to the time constant of the skin (See eq. (A2) in appendix A).

Application to Specific Conditions

For a given problem (a prescribed geometry or a set of geometric ratios and prescribed boundary and initial conditions), the results (the variation of the temperature and stress ratios with the time parameter)

may be applied to any material for various combinations of geometric size, aerodynamic heat-transfer coefficient, and joint conductivity. Once the type of material has been designated, the values of k, c, w, E, and α become fixed. Then, selection of a value of h determines the value of t_s or selection of t_s determines the value of h, as dictated by the aerodynamic heat-transfer parameter ht_s/k. The selected value of h can usually be attained under many aerodynamic conditions; these aerodynamic conditions must then be used to find both T_{AW} and T_0; the actual values of the temperatures may then be converted from the nondimensional temperature ratios. The values already selected for t_s and k dictate the value of the joint heat-transfer coefficient to be obtained from the ratio $h_j t_s/k$. When combined with the set of geometric ratios, the value of t_s determines the actual size of the structure. The values of T_{AW} and T_0, which are dependent upon the aerodynamic conditions, and the material properties establish the magnitudes of the stresses (converted from the stress ratios). The times for the converted values of the temperatures and stresses depend upon the aerodynamic heat-transfer coefficient, the material properties (c and w), and the skin thickness and are found from the time parameter $h\tau/cwt_s$. Thus, the nondimensional results for any one prescribed problem may be converted to many different results depending upon the selection of the aerodynamic heat-transfer coefficient, the material, the skin thickness, the joint conductivity, or the time. Any one or a combination of these quantities may dictate the magnitudes of the temperatures and stresses and the boundary conditions for an actual structure.

REFERENCES

1. Heldenfels, Richard R.: The Effect of Nonuniform Temperature Distributions on the Stresses and Distortions of Stiffened-Shell Structures. NACA TN 2240, 1950.

2. Soroka, Walter W.: Analog Methods in Computation and Simulation. McGraw-Hill Book Co., Inc., 1954.

3. Korn, Granino A., and Korn, Theresa M.: Electronic Analog Computers. First ed., McGraw-Hill Book Co., Inc., 1952.

4. Benscoter, Stanley U., and MacNeal, Richard H.: Introduction to Electrical-Circuit Analogies for Beam Analysis. NACA TN 2785, 1952.

5. Howe, R. M.: Application of Difference Techniques to Heat Flow Problems Using the Electronic Differential Analyzer. AIR-10, Project 2115-3-T (Contract No. DA-20-018-ORD-21811), Eng. Res. Inst., Univ. of Michigan, May 1954.

6. Anon.: Working Data for Carpenter Stainless and Heat Resisting Steels. The Carpenter Steel Co. (Reading, Pa.), c.1952.

7. Barzelay, Martin E., Tong, Kin Nee, and Hollo, George: Thermal Conductance of Contacts in Aircraft Joints. NACA TN 3167, 1954.

8. Timoshenko, S.: Theory of Elasticity. First ed., McGraw-Hill Book Co., Inc., 1934, pp. 208-209.

9. McAdams, William H.: Heat Transmission. Second ed., McGraw-Hill Book Co., Inc., 1942, p. 23.

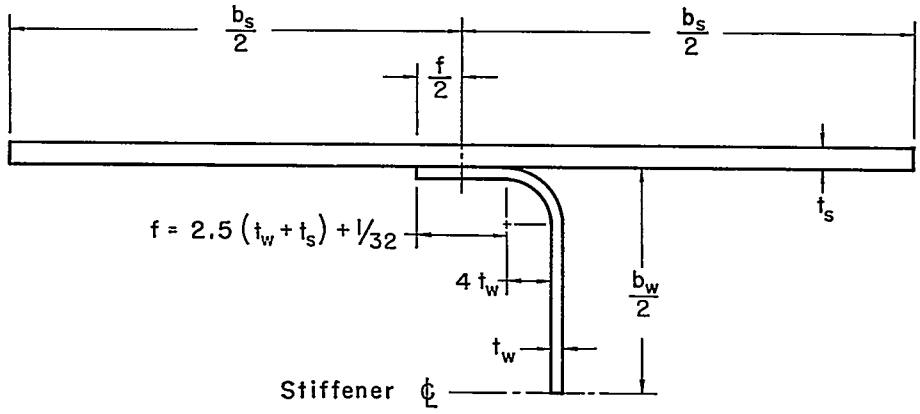

Figure 1.- Dimensions and symbols for one-half of symmetrical skin-stiffener geometry.

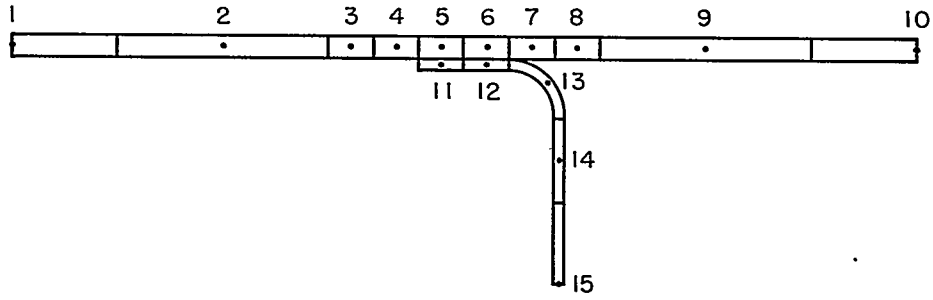

Figure 2.- Division of skin-stiffener geometry for analog calculations. $b_s/t_s = 40$.

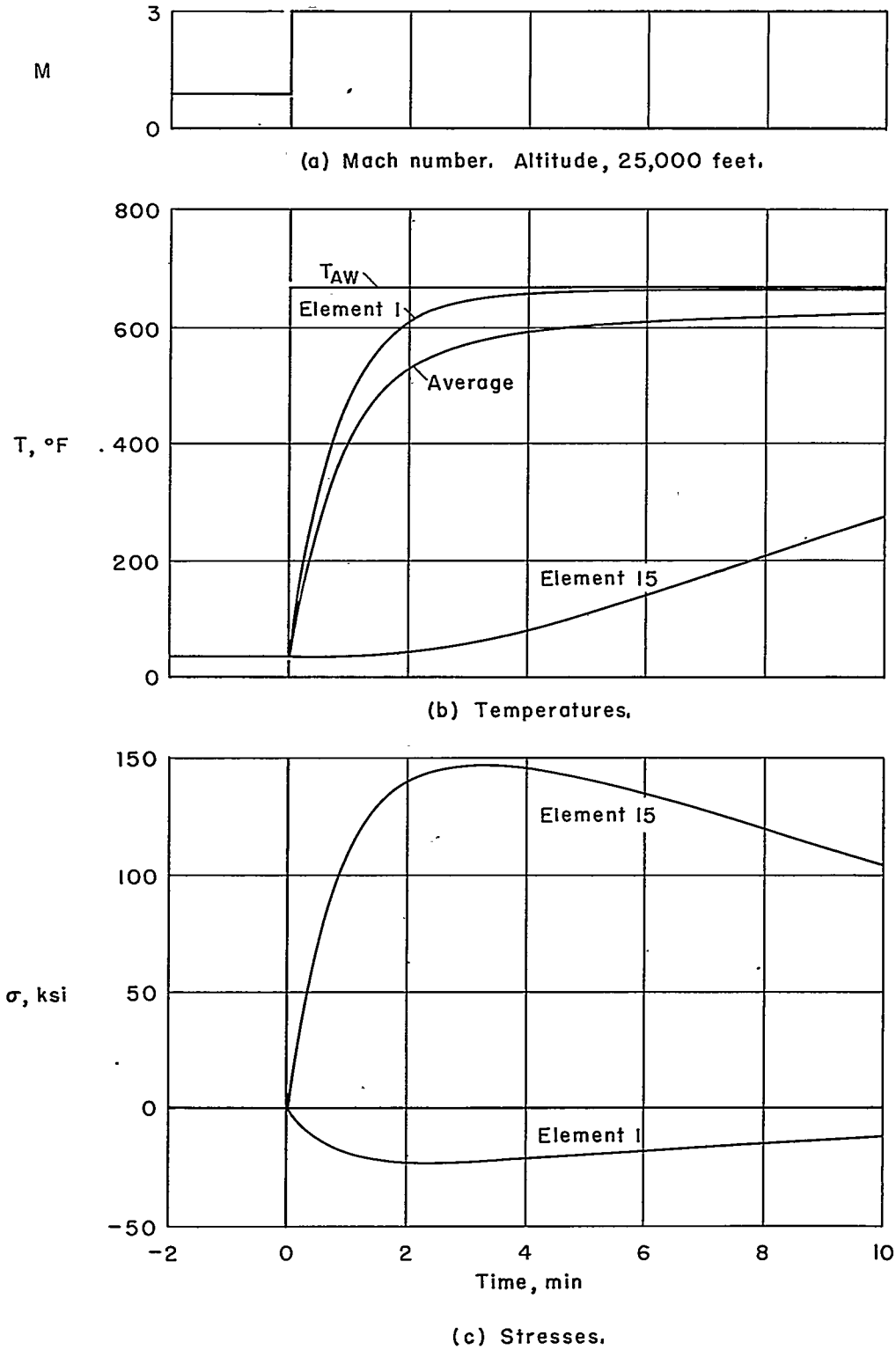

(a) Mach number. Altitude, 25,000 feet.

(b) Temperatures.

(c) Stresses.

Figure 3.- Flight history and temperature and stress histories for illustrative problem.

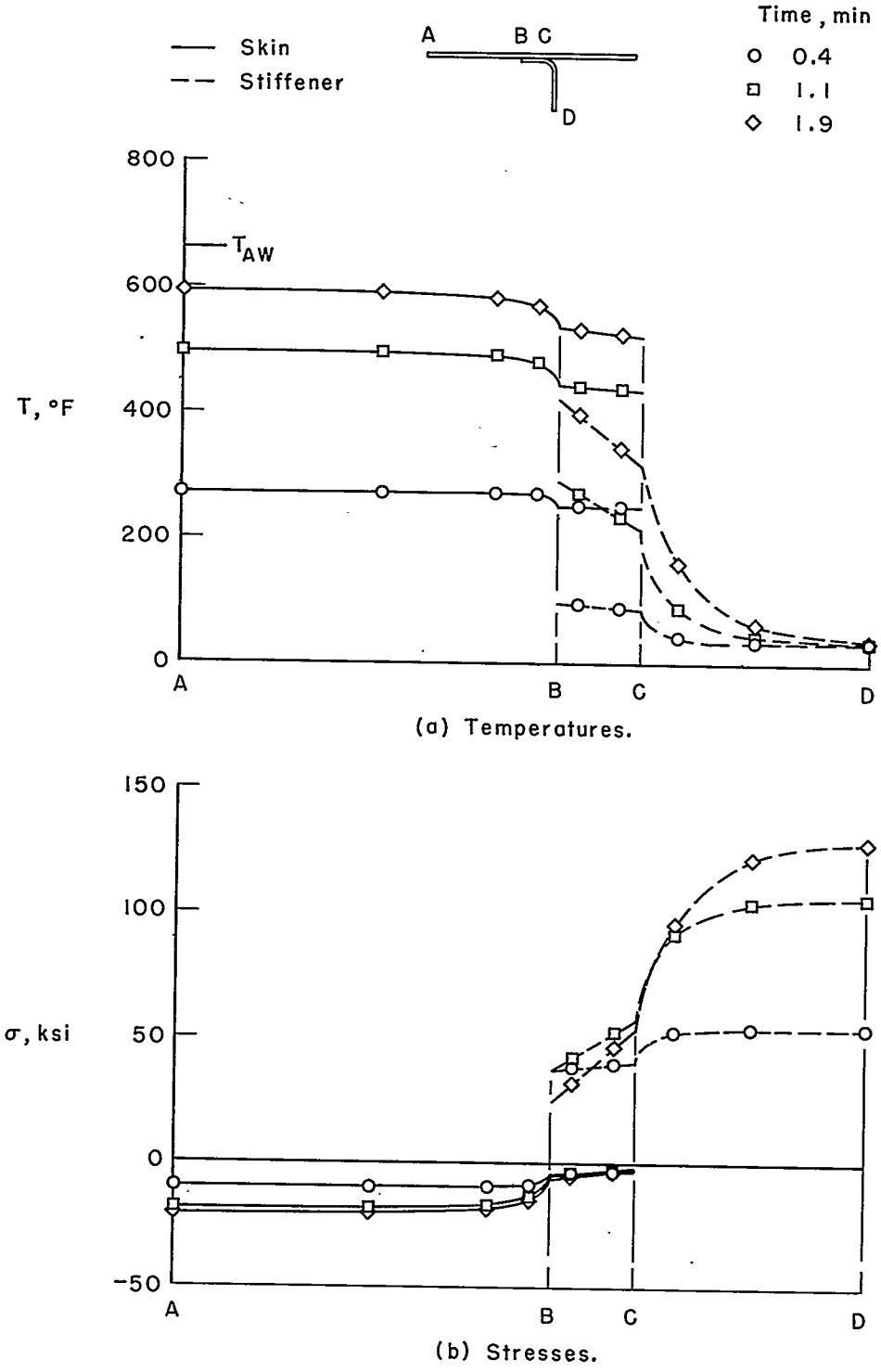

Figure 4.- Temperature and stress distributions for illustrative problem.

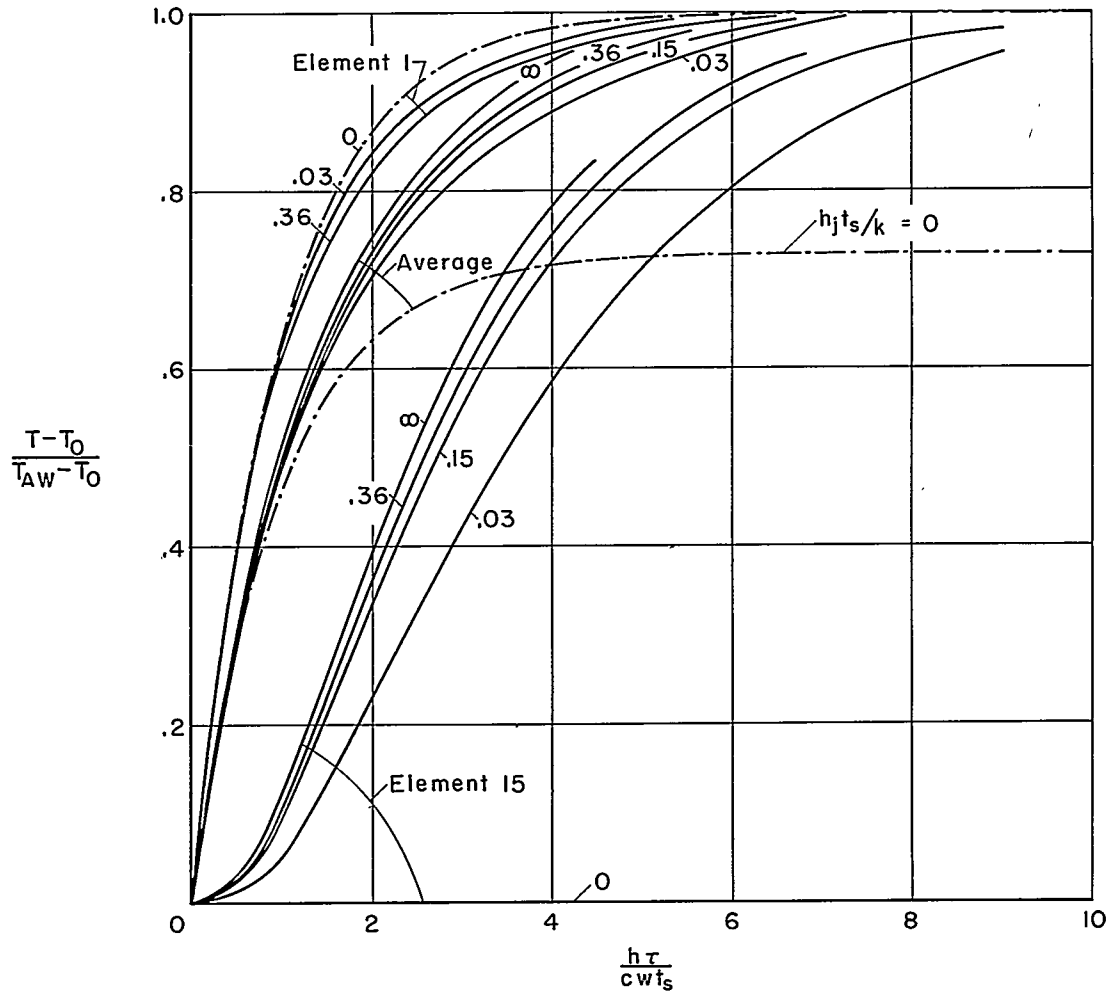

(a) Temperatures.

Figure 5.- The effect on the temperatures and stresses of varying the joint conductivity parameter $h_j t_s/k$. $b_s/t_s = 20$ and $ht_s/k = 0.02$.

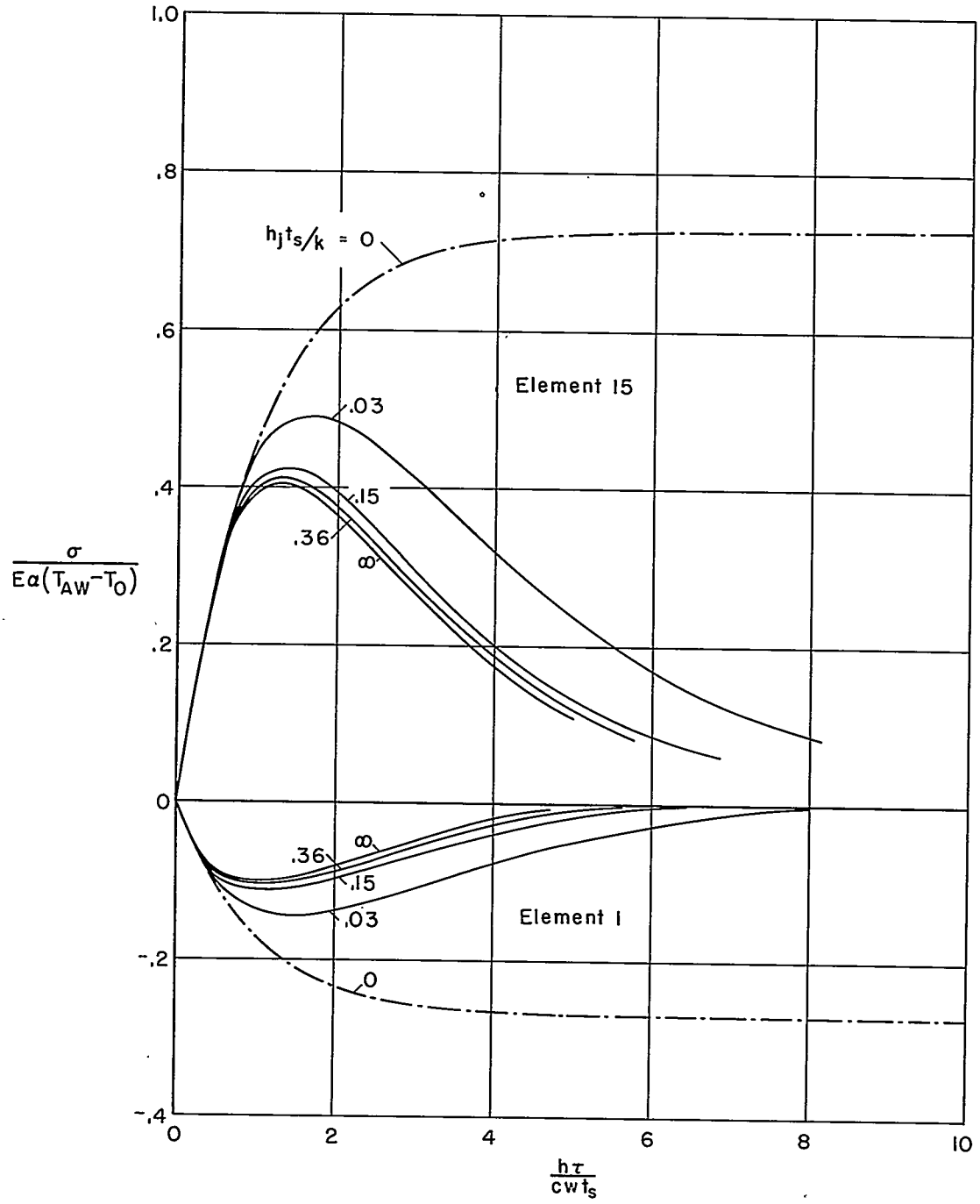

(b) Stresses.

Figure 5.- Concluded.

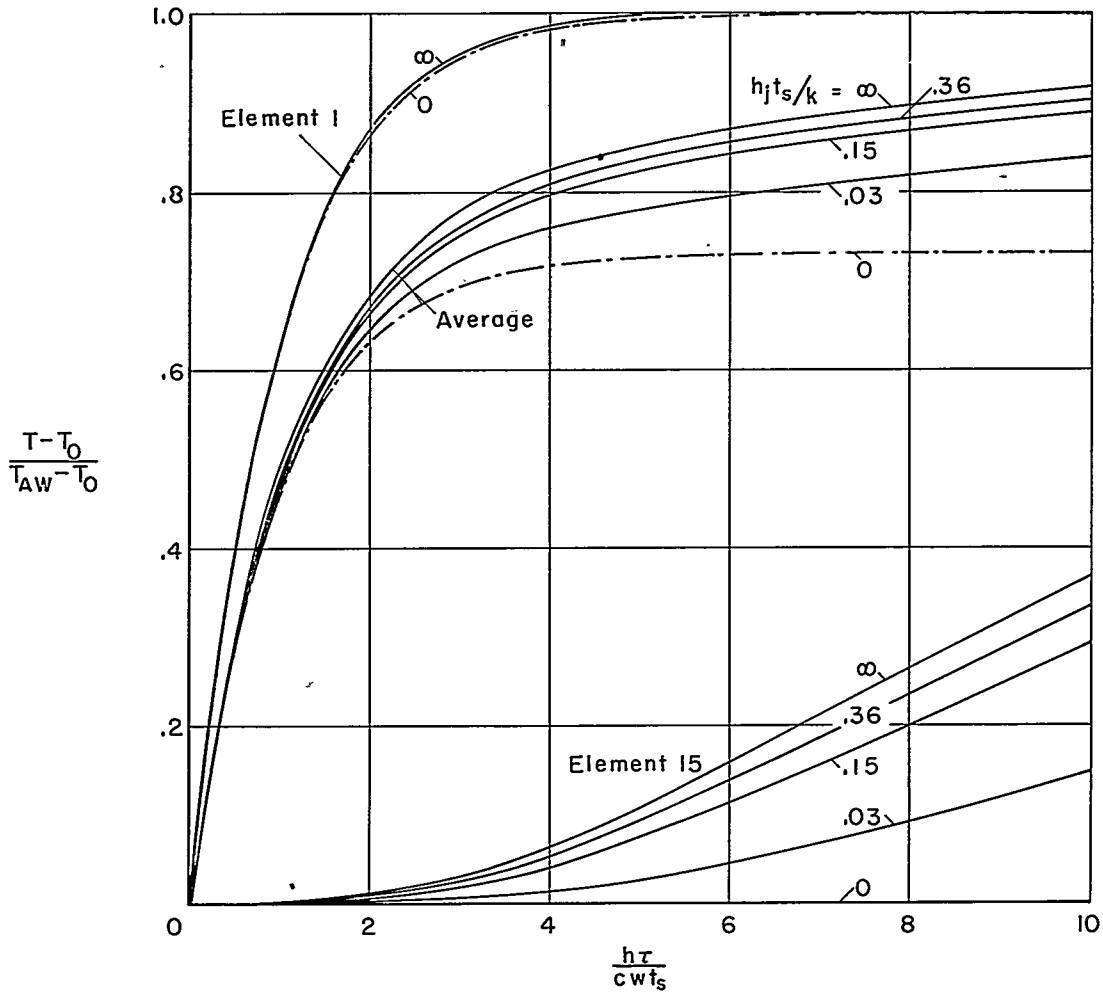

(a) Temperatures.

Figure 6.- The effect on the temperatures and stresses of varying the joint conductivity parameter $h_j t_s/k$. $b_s/t_s = 20$ and $ht_s/k = 0.2$.

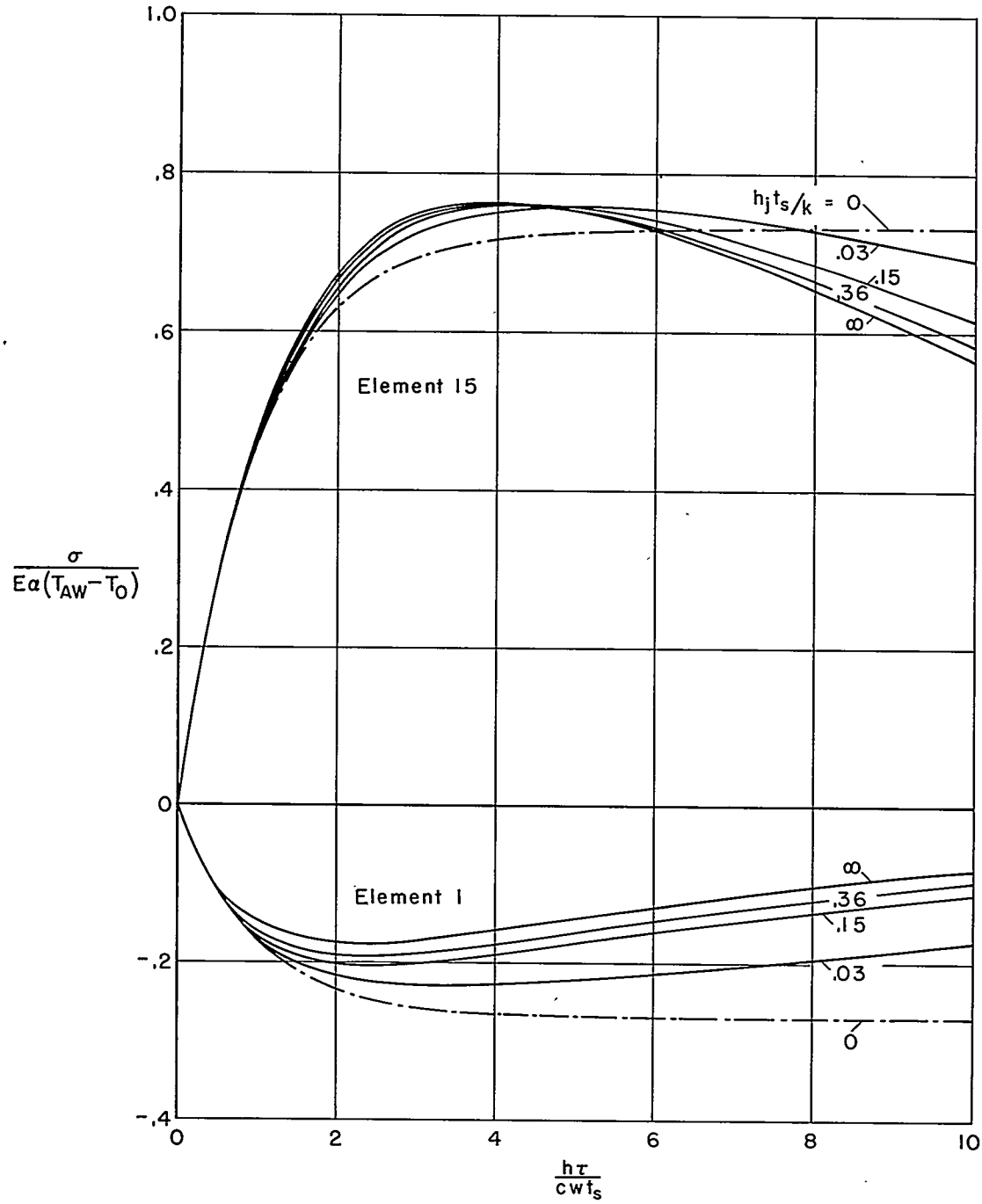

(b) Stresses.

Figure 6.- Concluded.

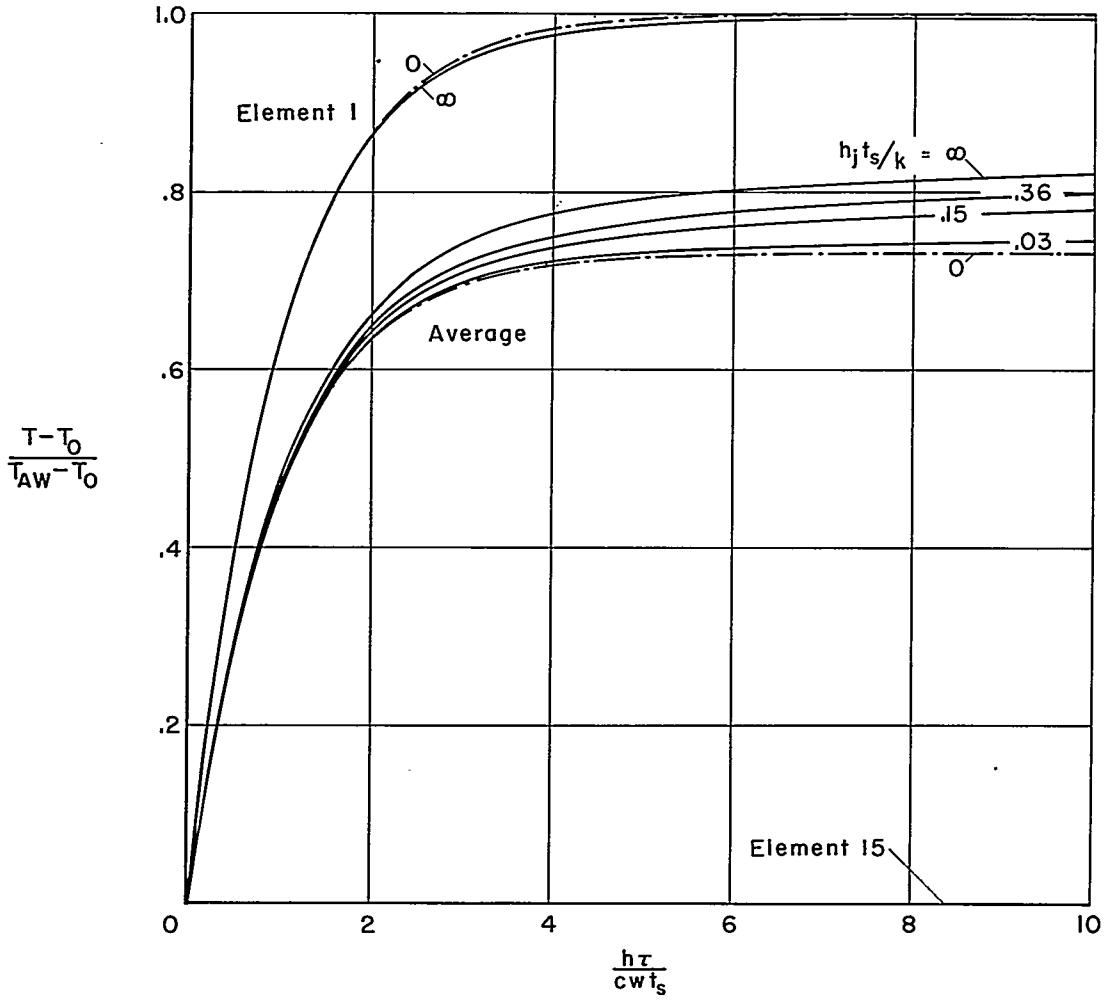

(a) Temperatures.

Figure 7.- The effect on the temperatures and stresses of varying the joint conductivity parameter $h_j t_s/k$. $b_s/t_s = 20$ and $ht_s/k = 2$.

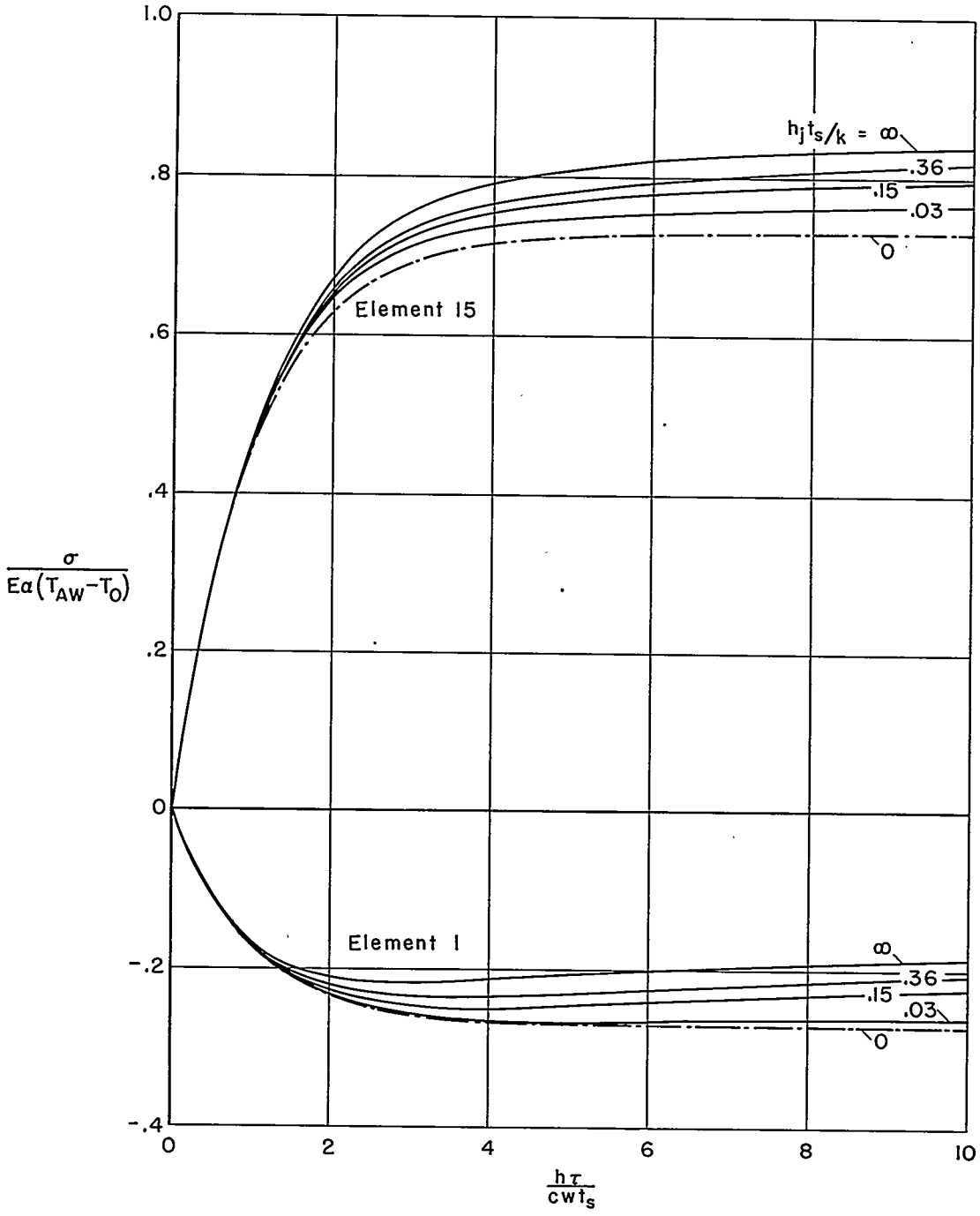

(b) Stresses.

Figure 7.- Concluded.

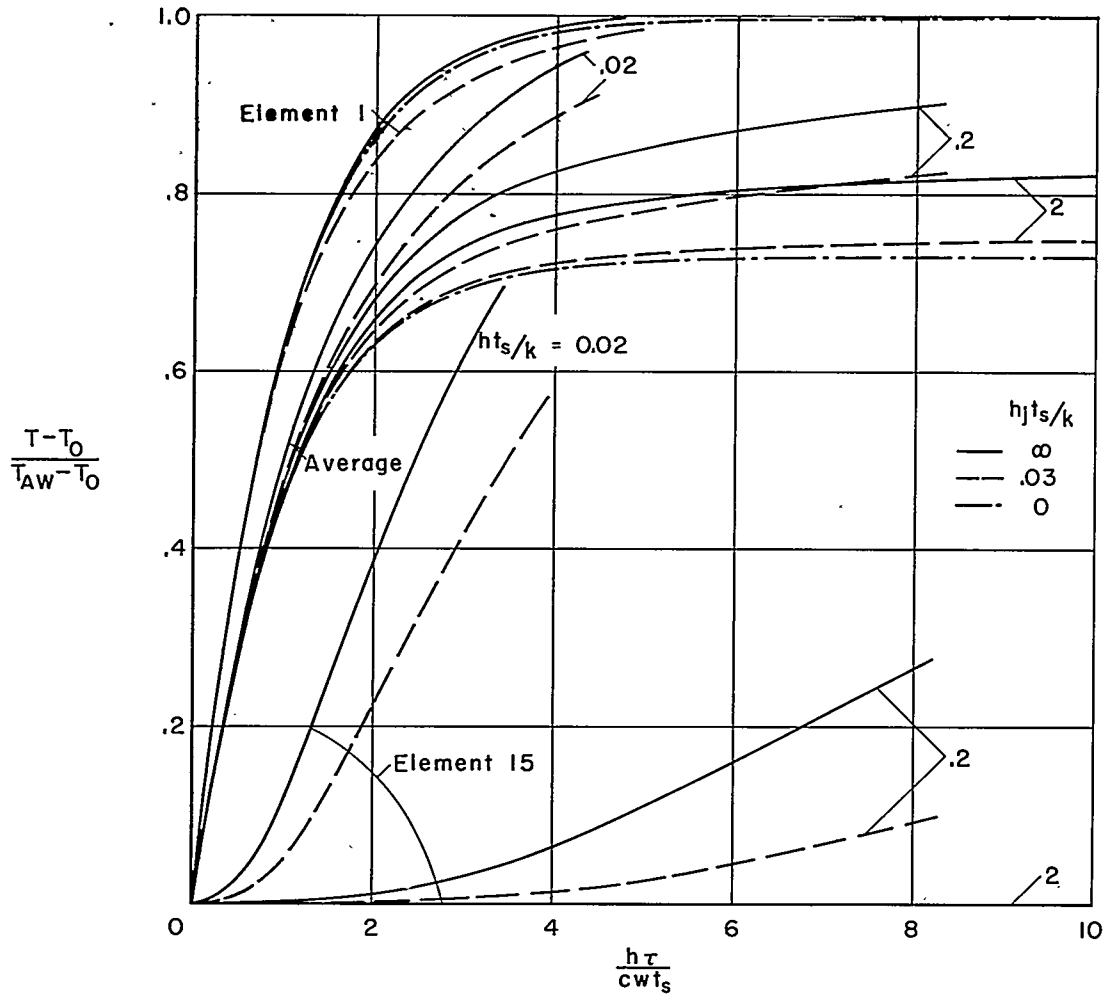

(a) Temperatures.

Figure 8.- The effect on the temperatures and stresses of varying h_jt_s/k and ht_s/k. $b_s/t_s = 20$.

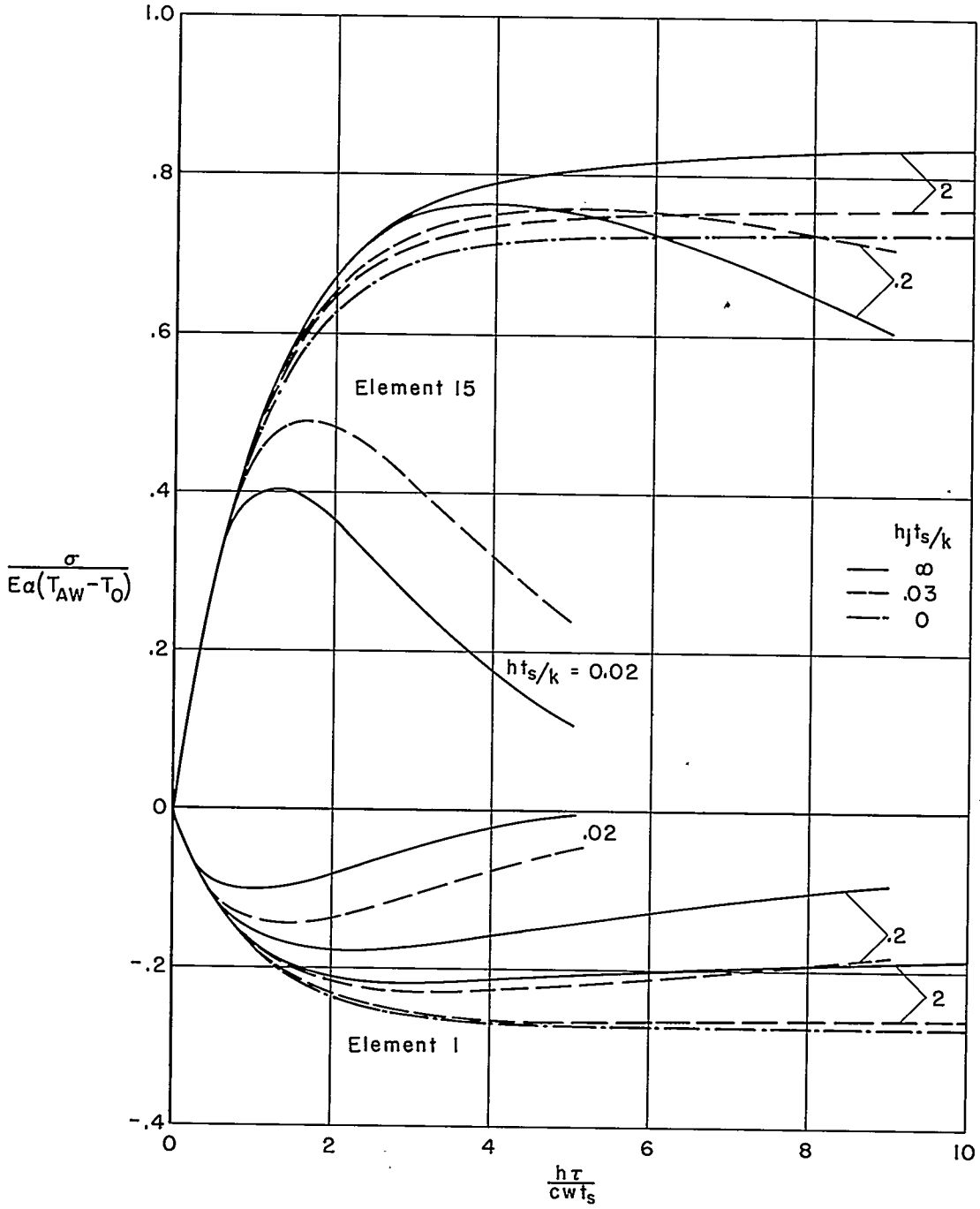

(b) Stresses.

Figure 8.- Concluded.

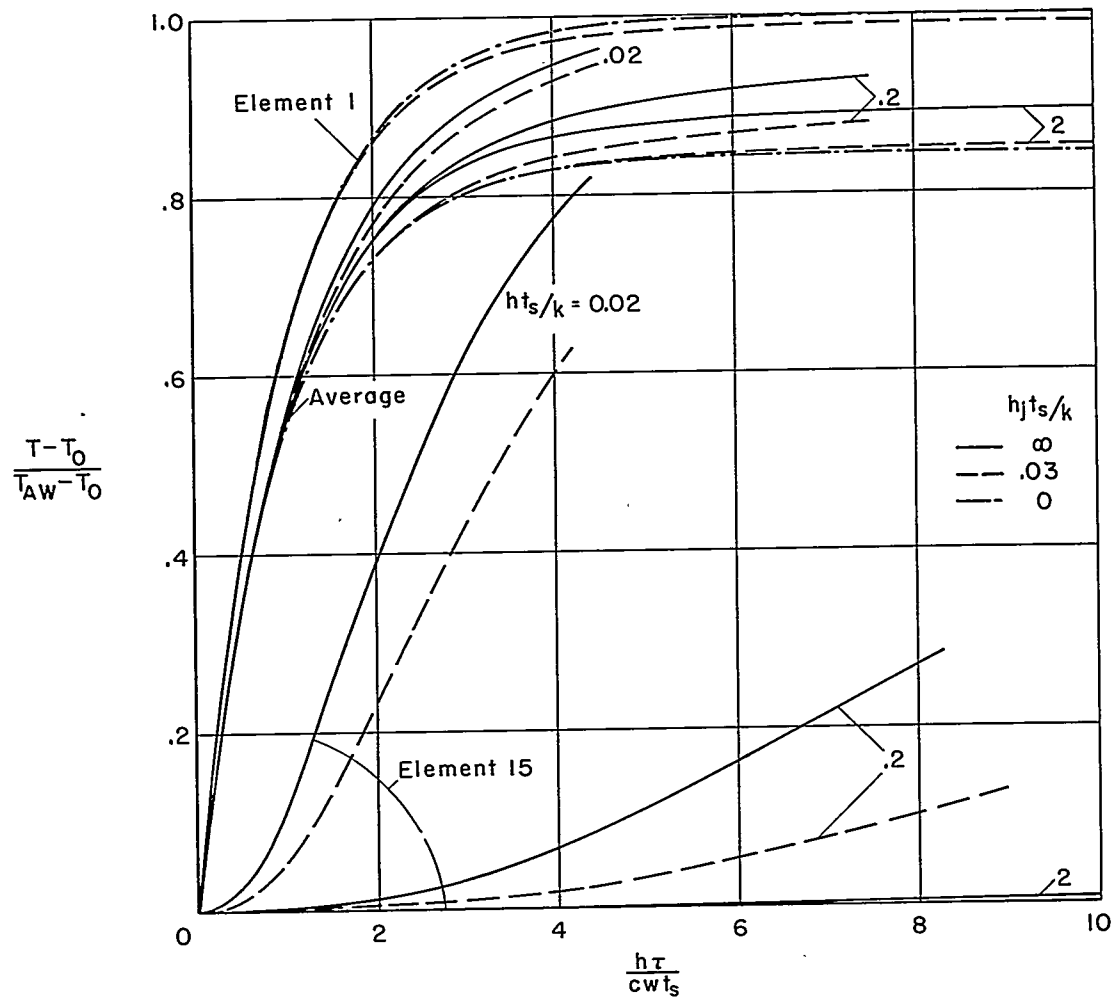

(a) Temperatures.

Figure 9.- The effect on the temperatures and stresses of varying $h_j t_s/k$ and ht_s/k. $b_s/t_s = 40$.

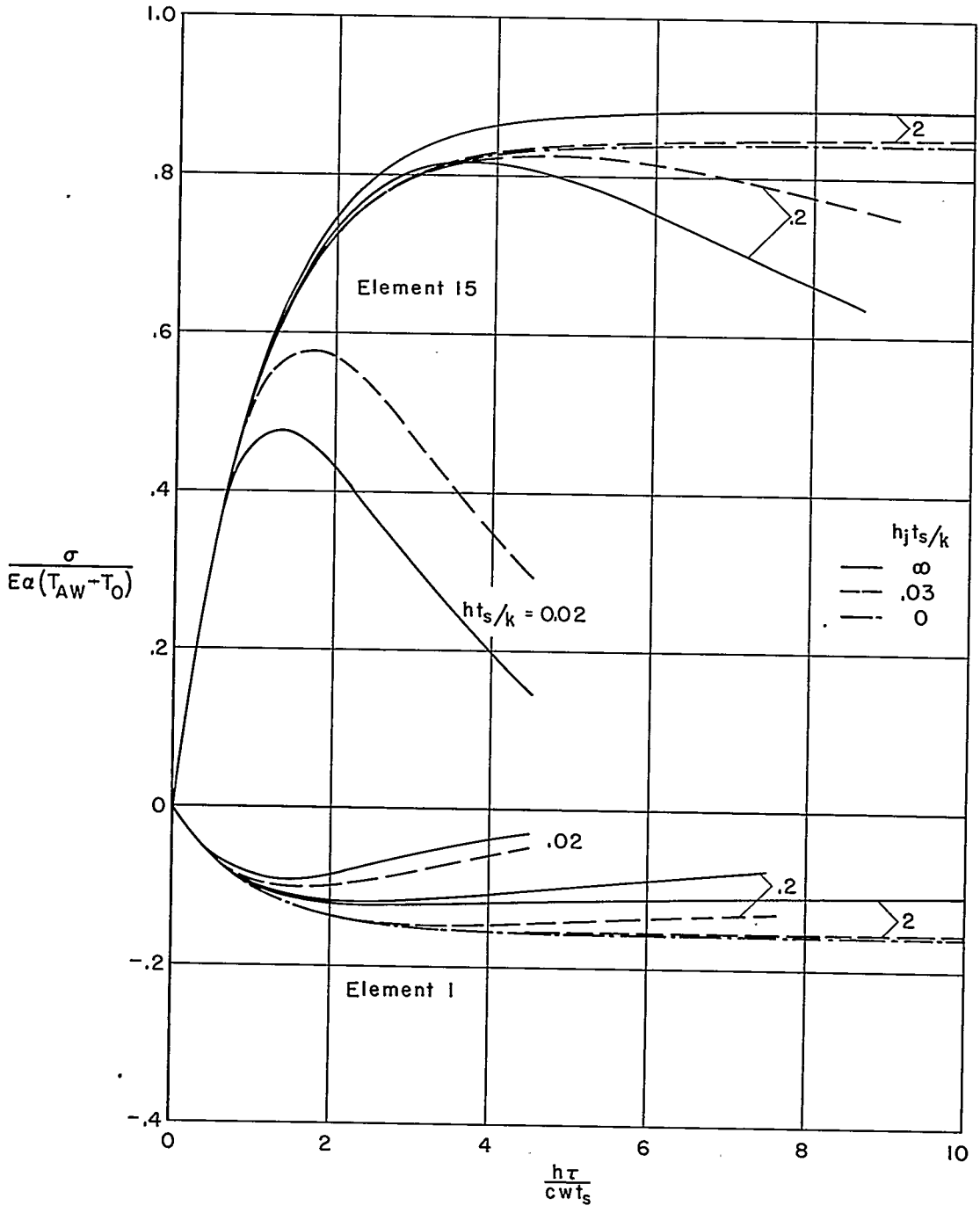

(b) Stresses.

Figure 9.- Concluded.

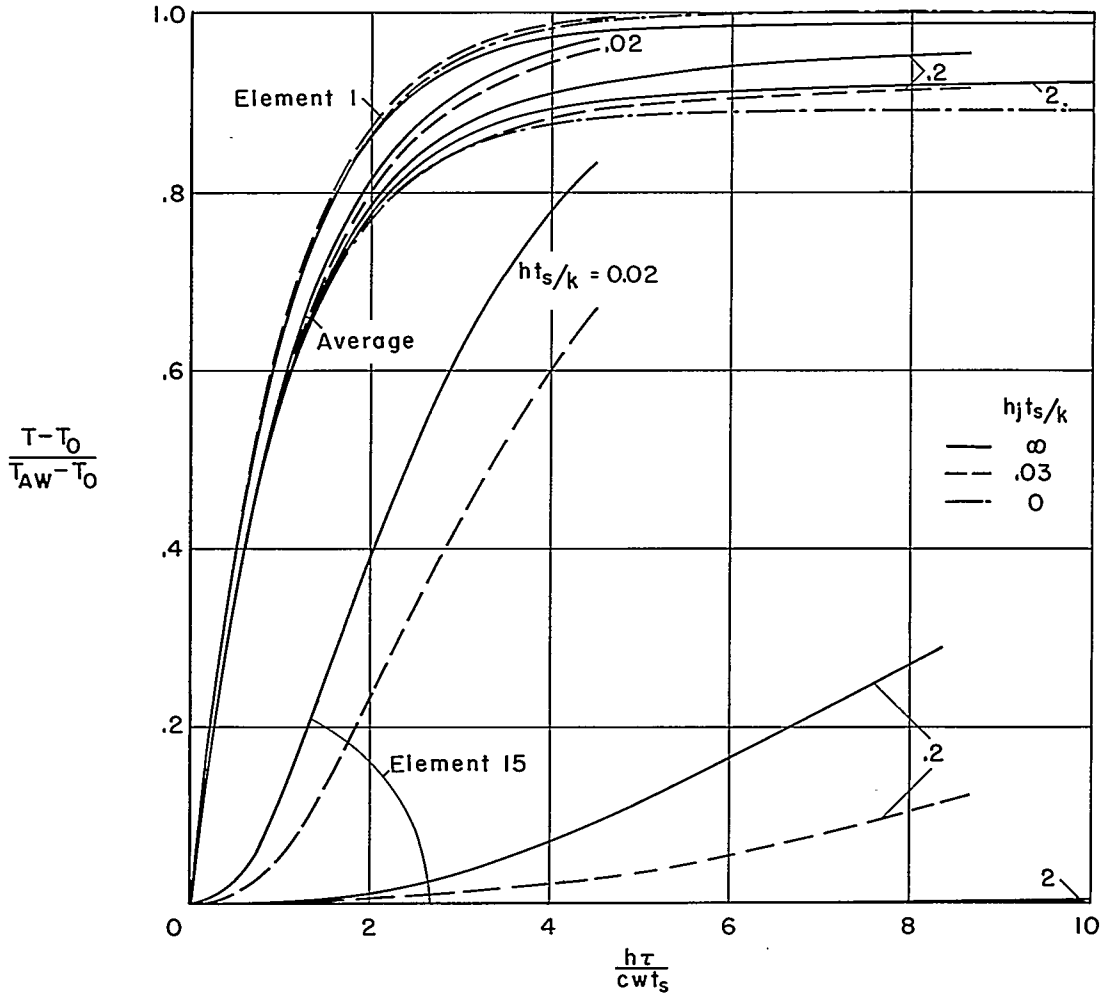

(a) Temperatures.

Figure 10.- The effect on the temperatures and stresses of varying $h_j t_s/k$ and ht_s/k. $b_s/t_s = 60$.

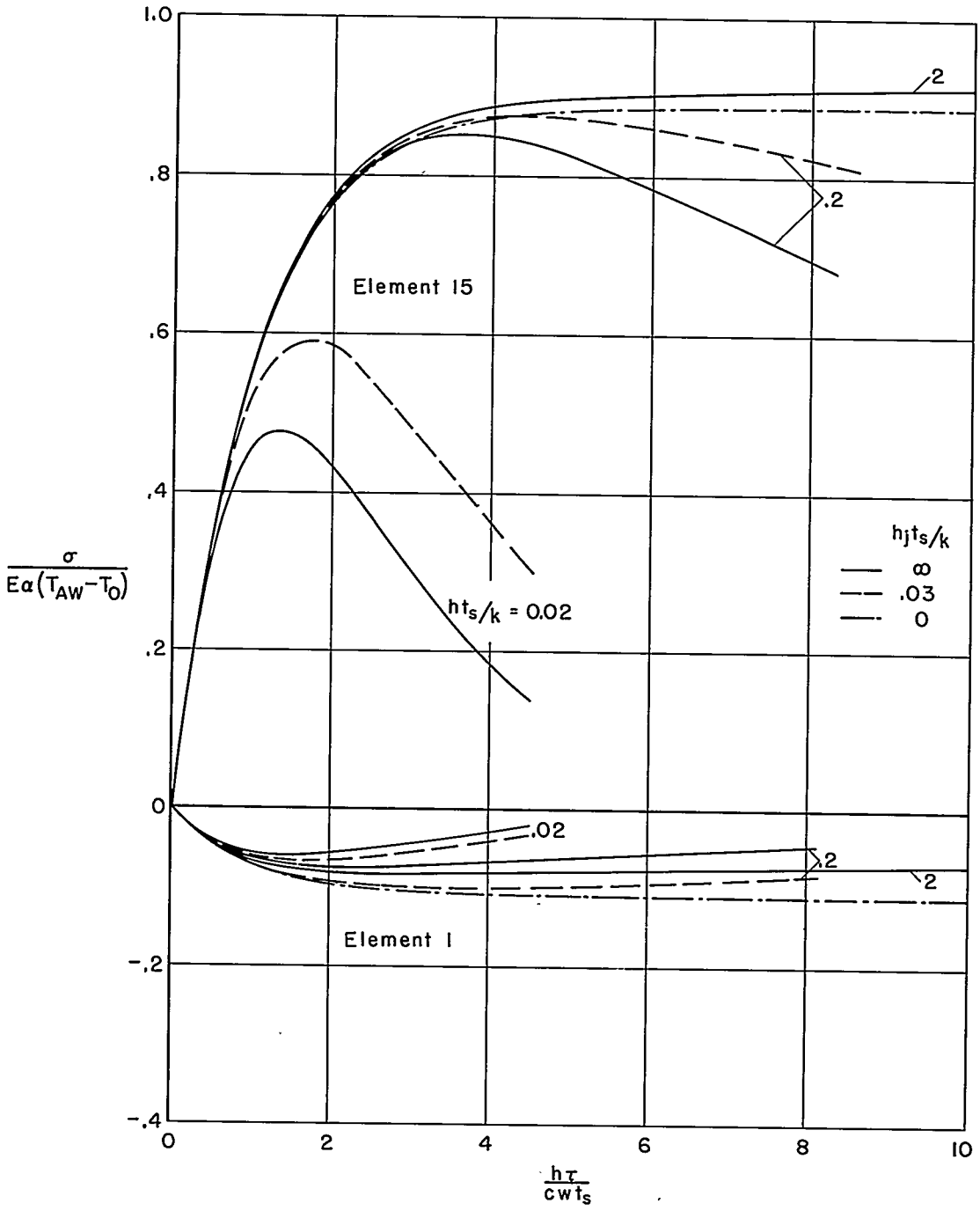

(b) Stresses.

Figure 10.- Concluded.

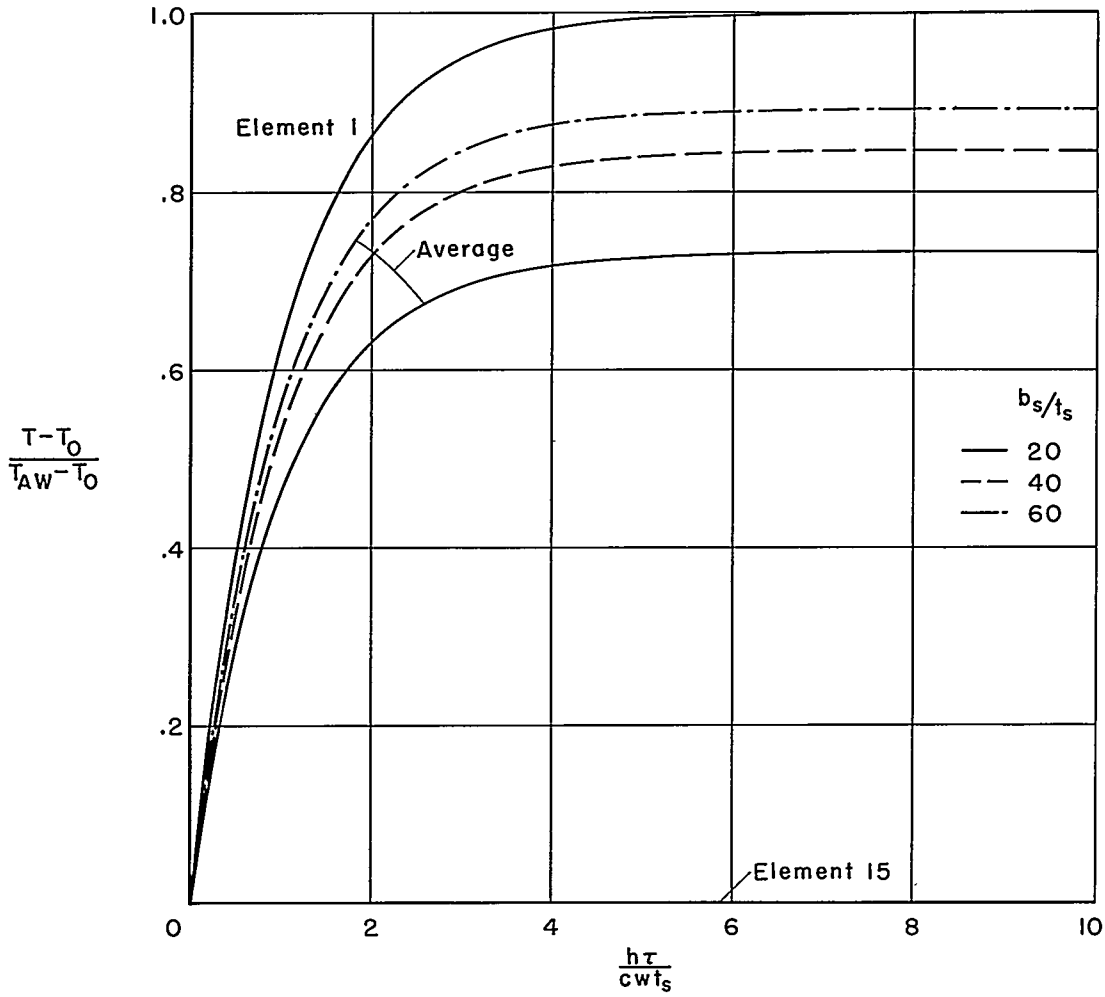

(a) Temperatures.

Figure 11.- The effect on the temperatures and stresses of varying the geometric ratio b_s/t_s. $ht_s/k = 0.2$ and $h_j t_s/k = 0$.

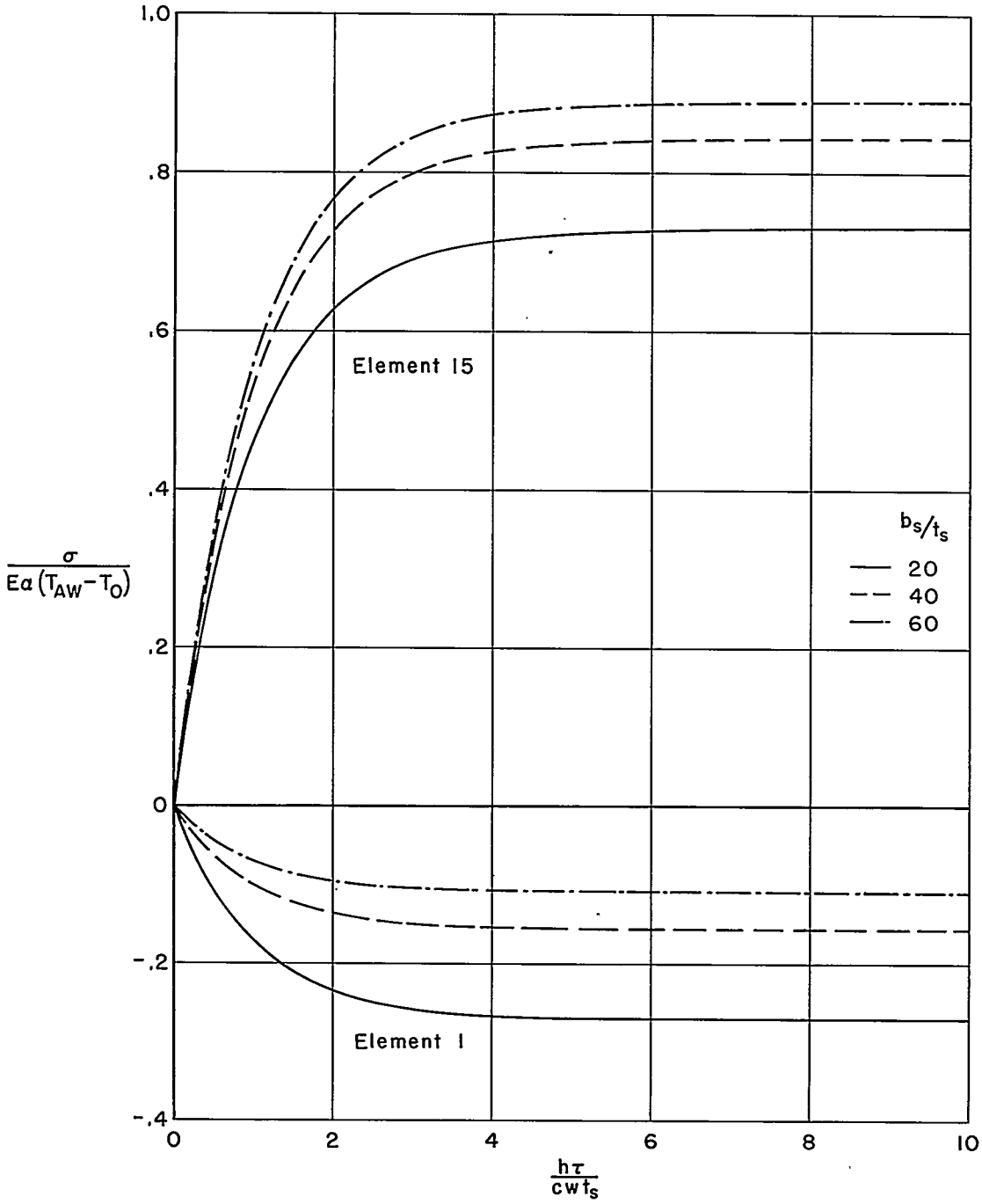

(b) Stresses.

Figure 11.- Concluded.

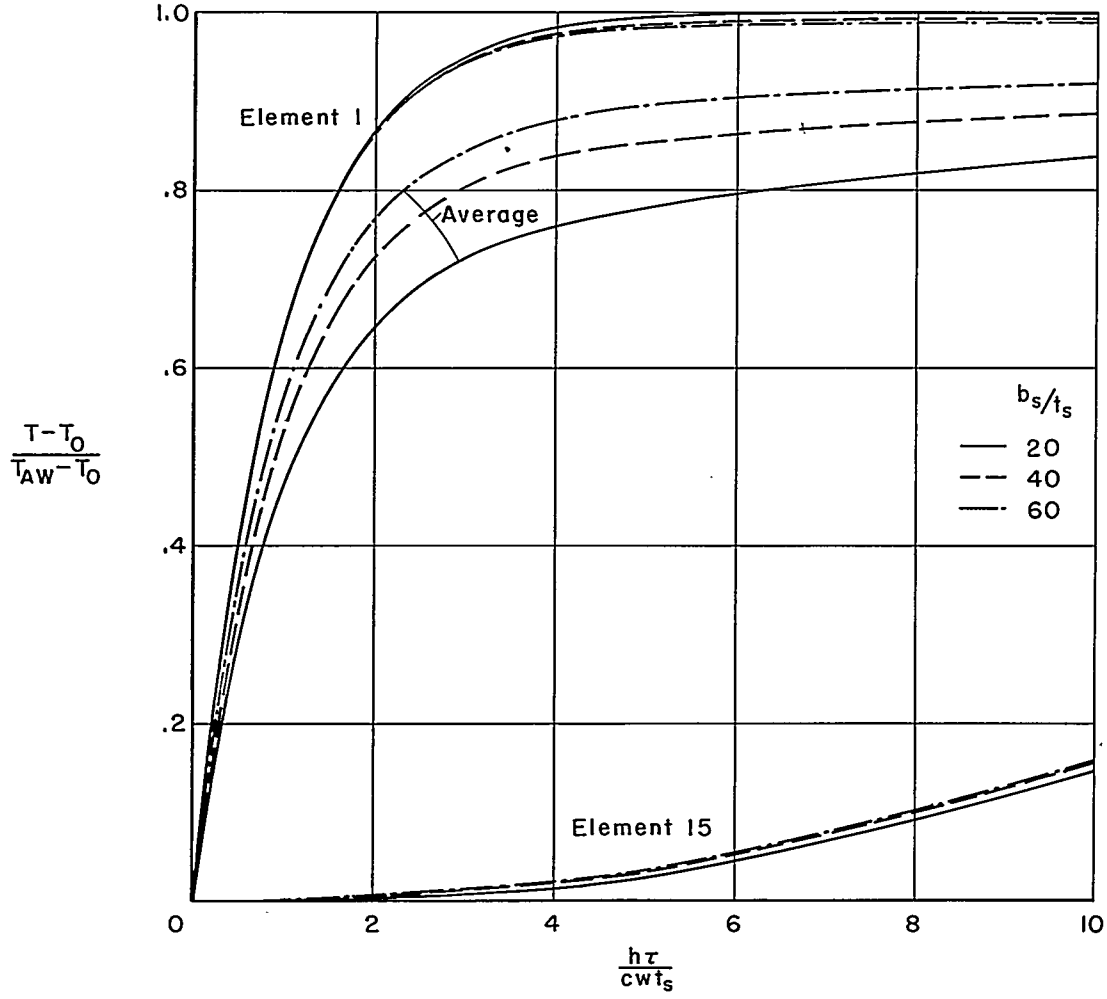

(a) Temperatures.

Figure 12.- The effect on the temperatures and stresses of varying the geometric ratio b_s/t_s. $ht_s/k = 0.2$ and $h_j t_s/k = 0.03$.

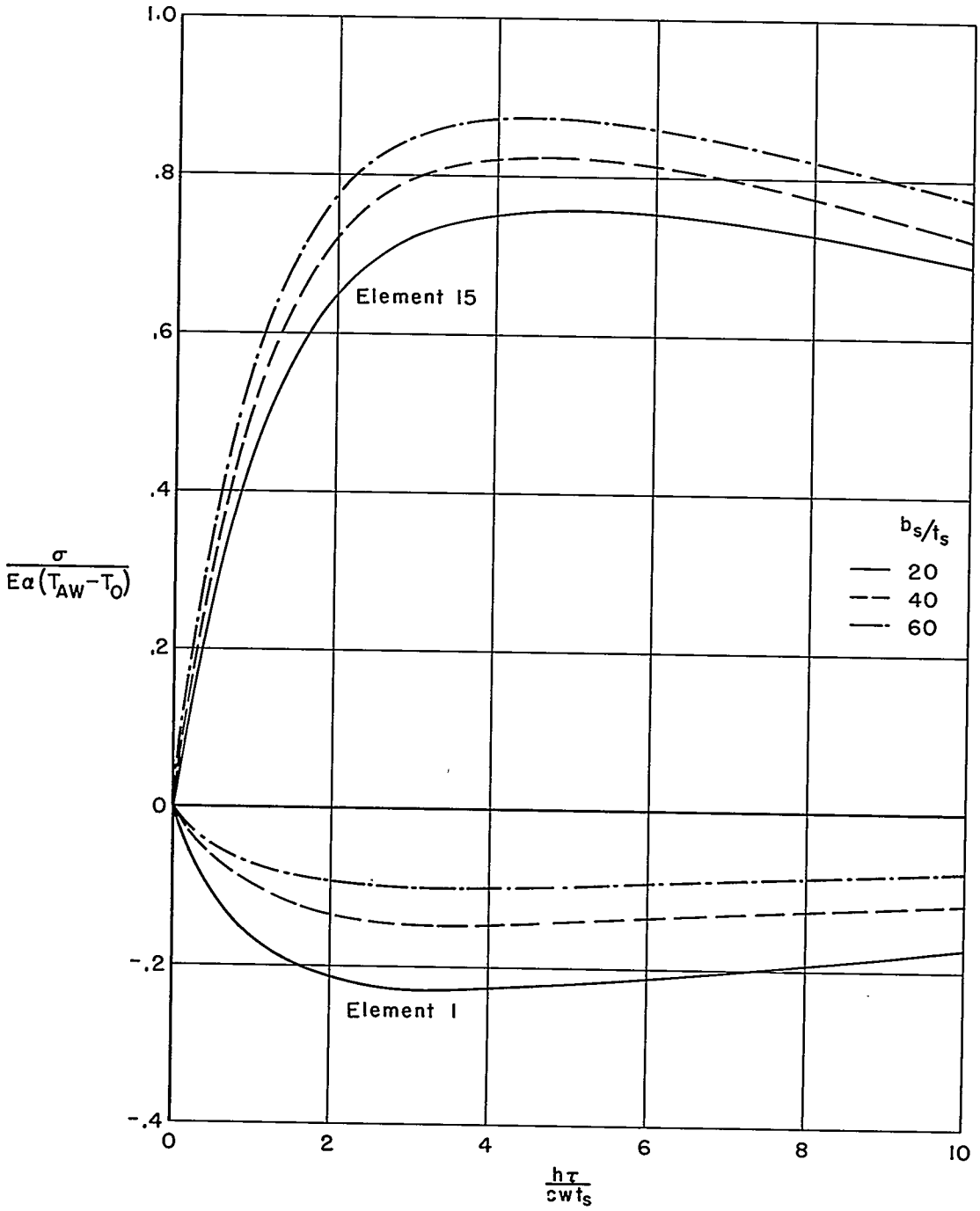

(b) Stresses.

Figure 12.- Concluded.

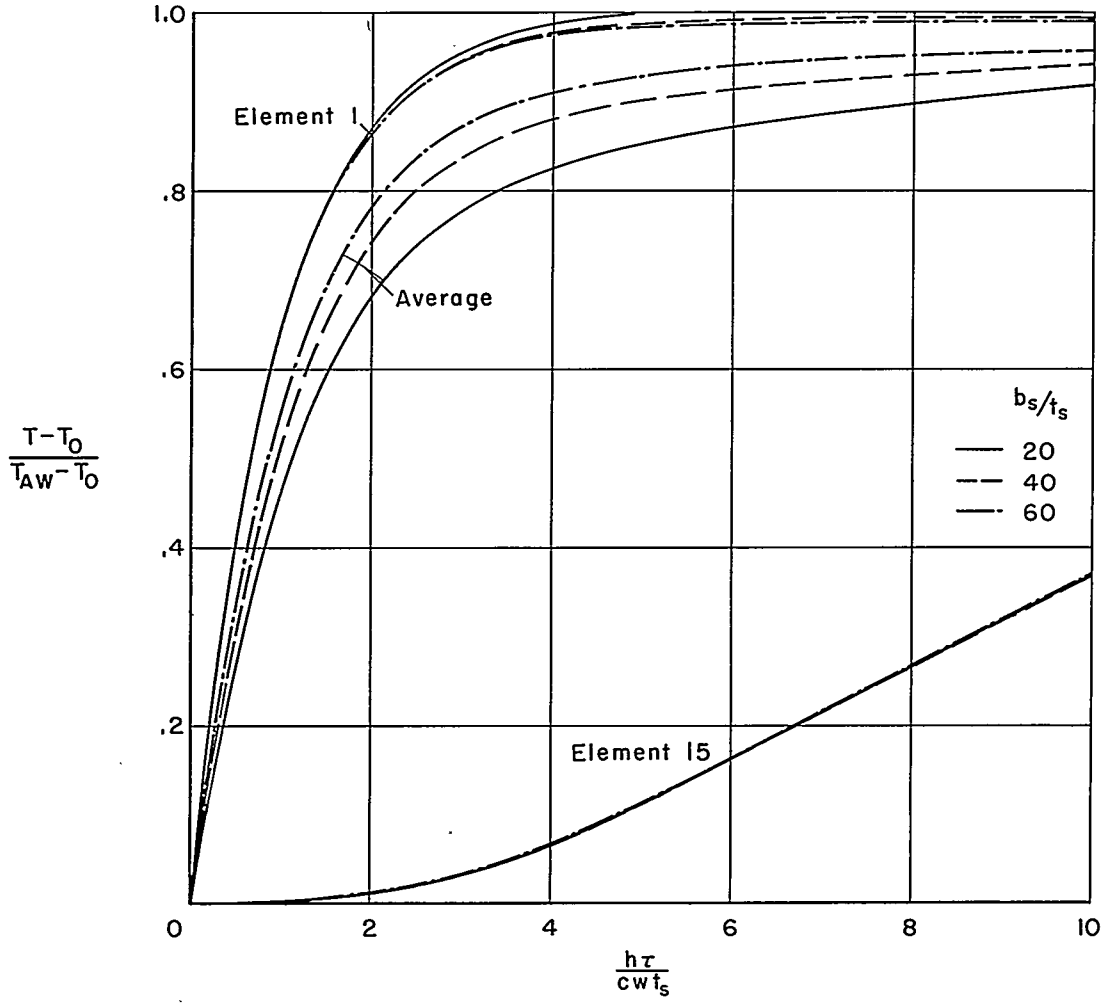

(a) Temperatures.

Figure 13.- The effect on the temperatures and stresses of varying the geometric ratio b_s/t_s. $ht_s/k = 0.2$ and $h_j t_s/k = \infty$.

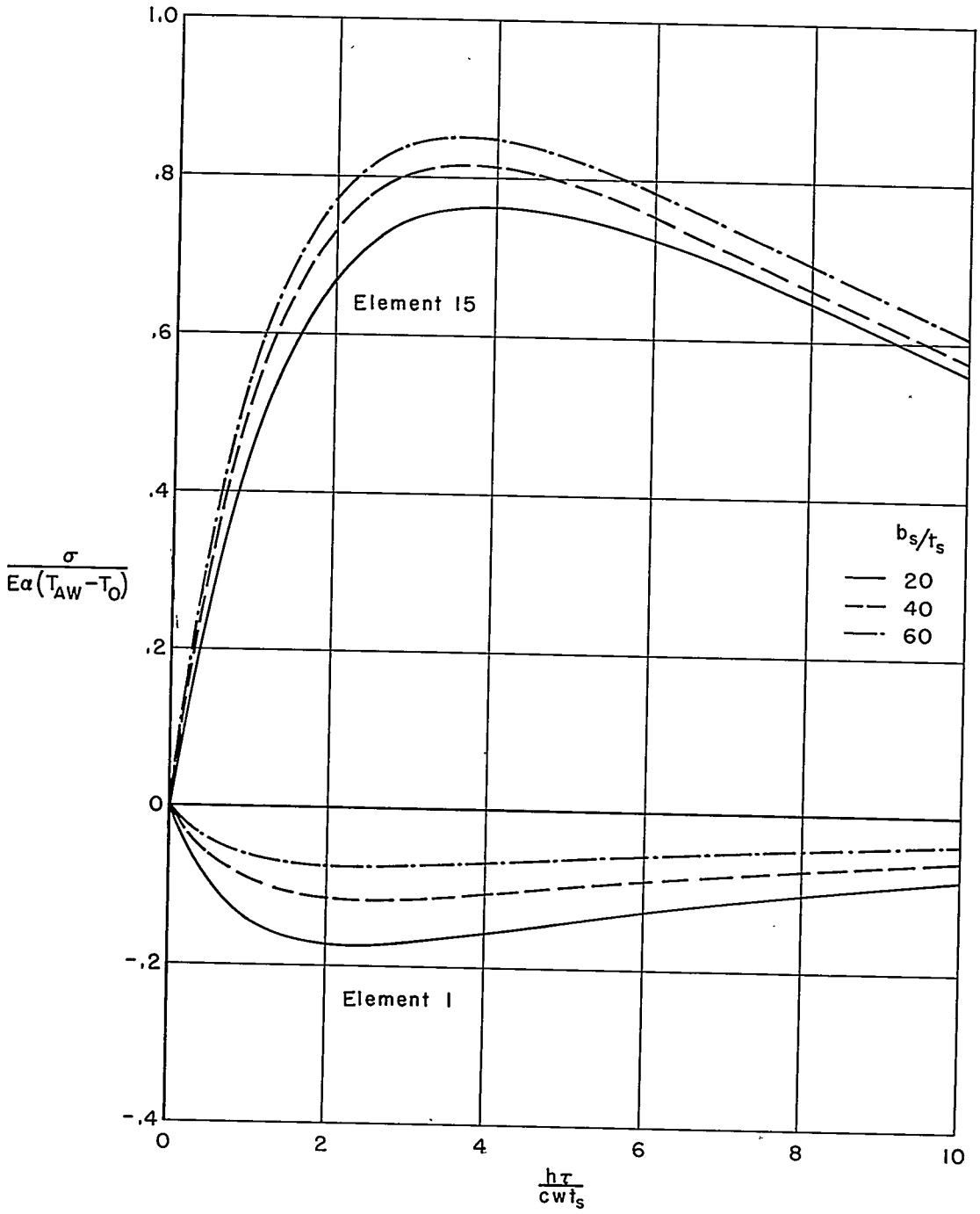

(b) Stresses.

Figure 13.- Concluded.

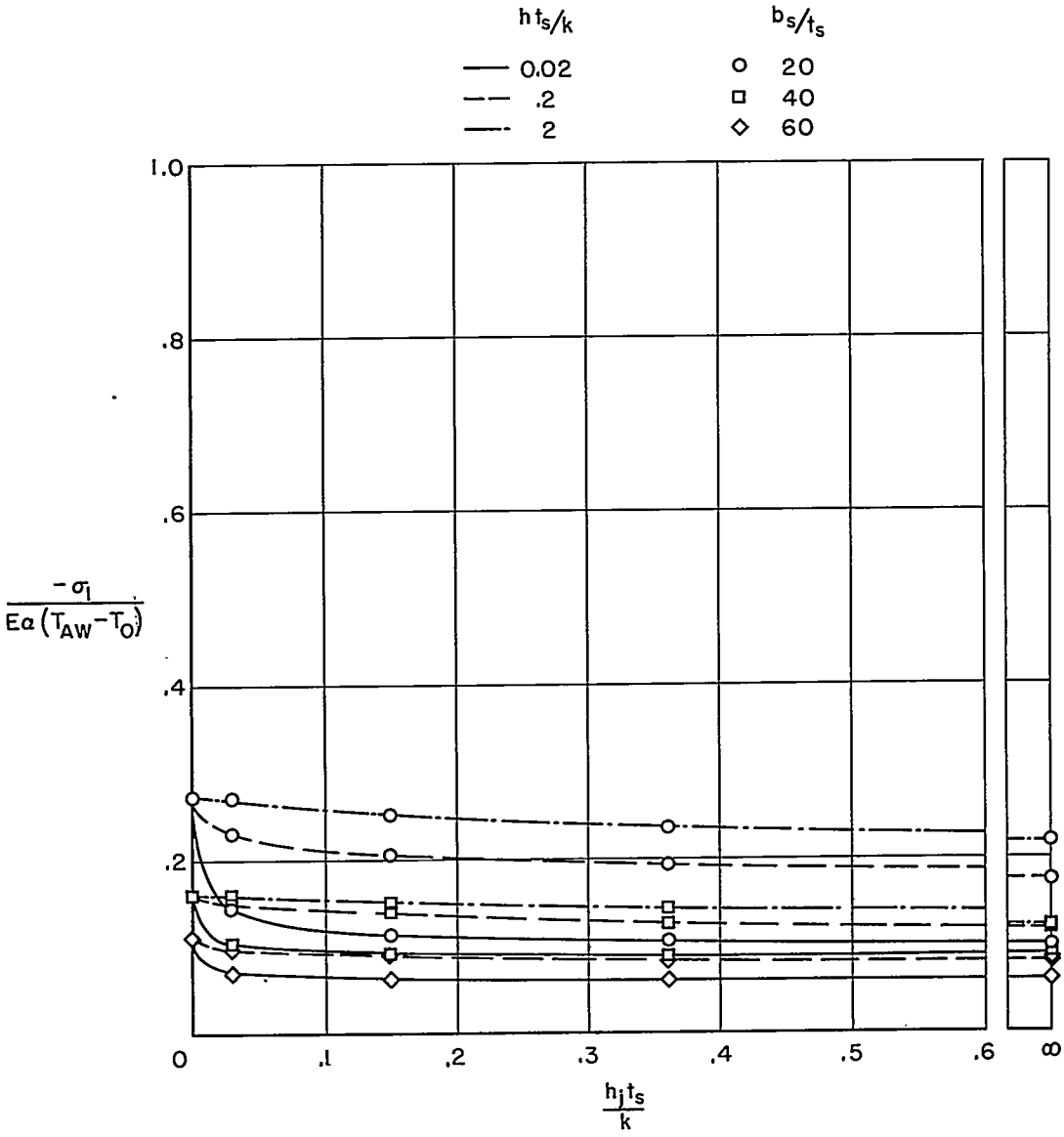

(a) Peak skin stress ratio.

Figure 14.- Variation of peak skin stress ratio and time parameter with $h_j t_s/k$.

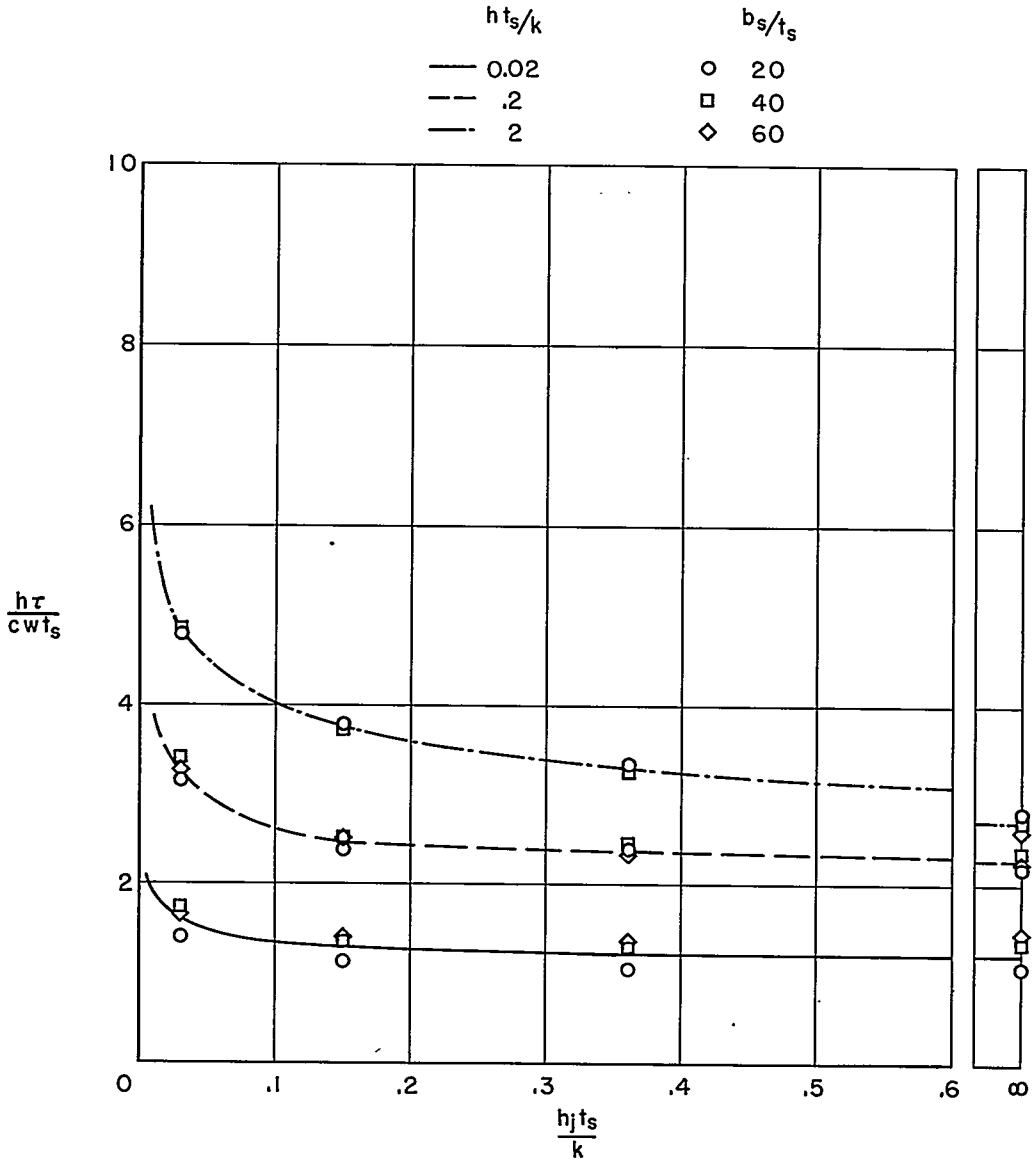

(b) Time parameter.

Figure 14.- Concluded.

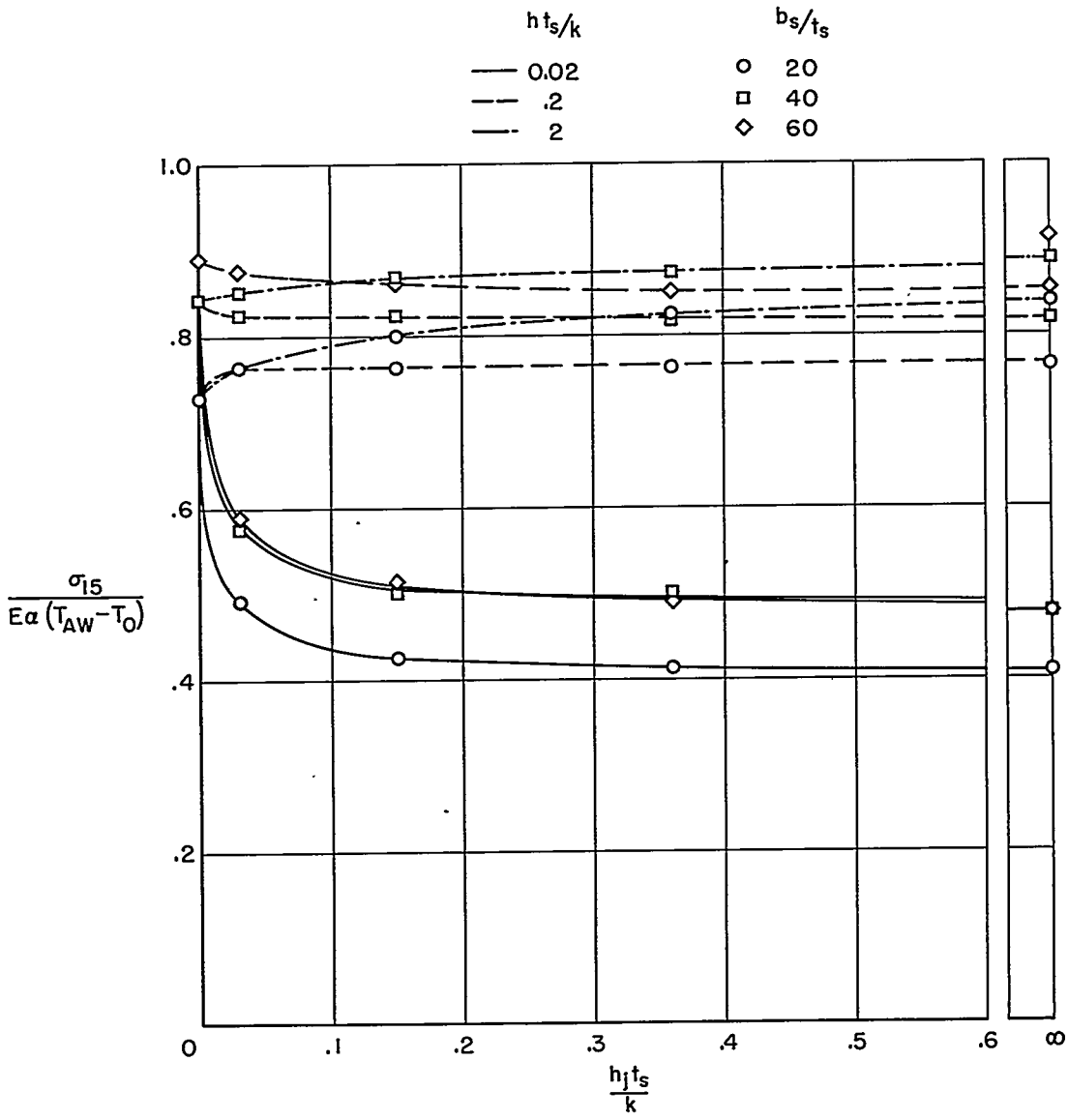

(a) Peak stiffener stress ratio.

Figure 15.- Variation of peak stiffener stress ratio and time parameter with $h_j t_s/k$.

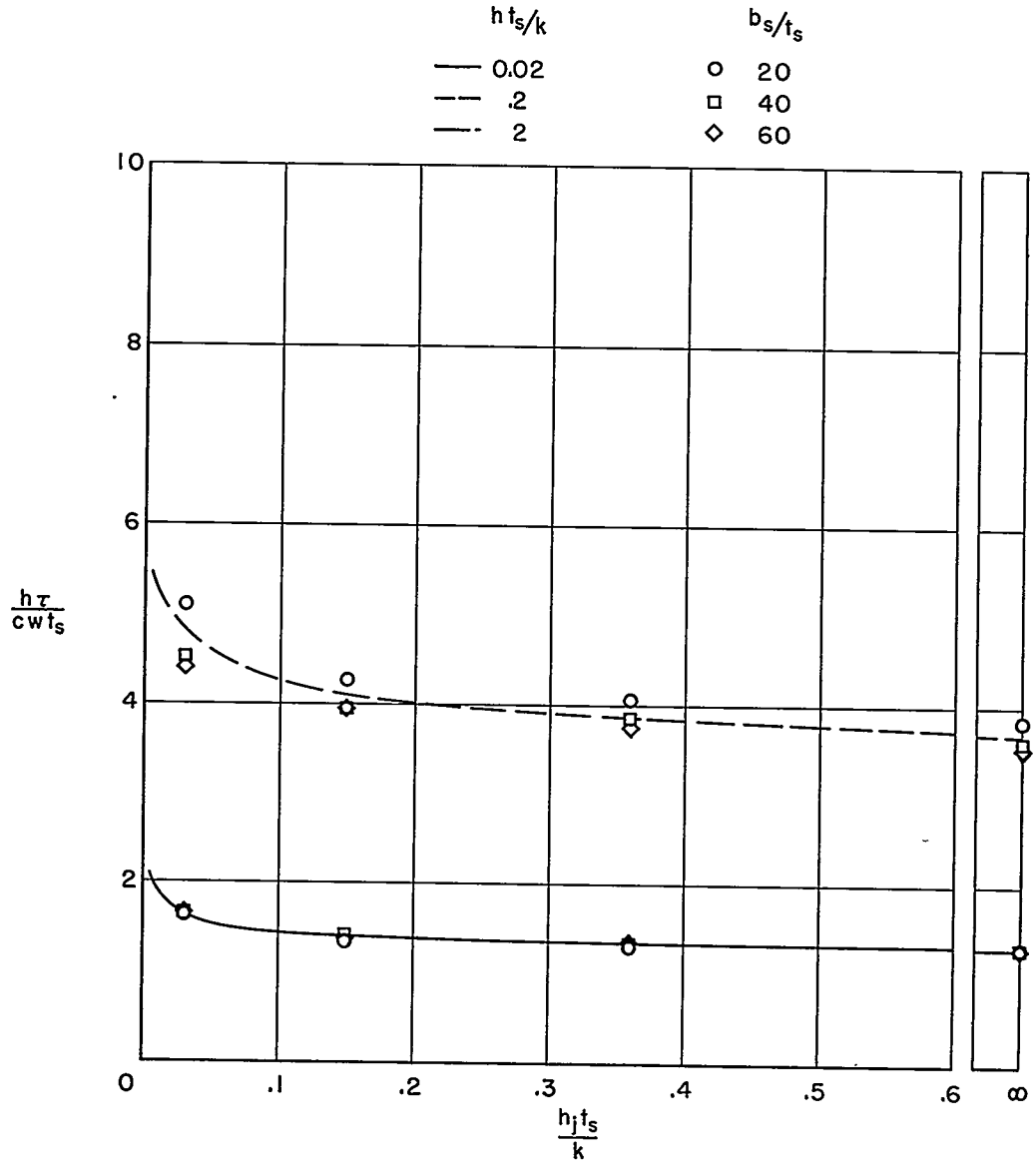

(b) Time parameter.

Figure 15.- Concluded.

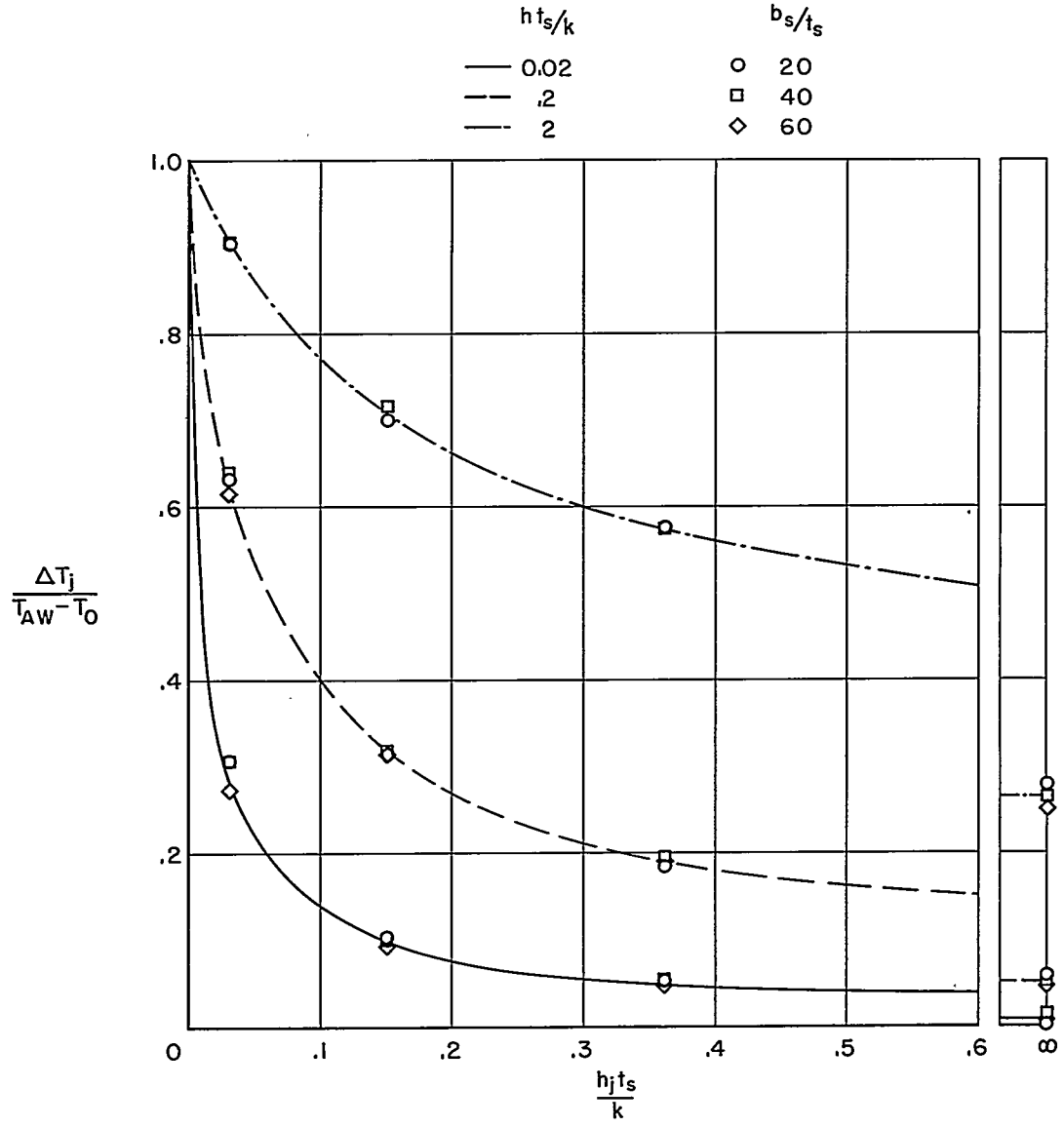

(a) Maximum temperature-ratio drop across joint.

Figure 16.- Variation of maximum temperature-ratio drop across joint and time parameter with $h_j t_s/k$.

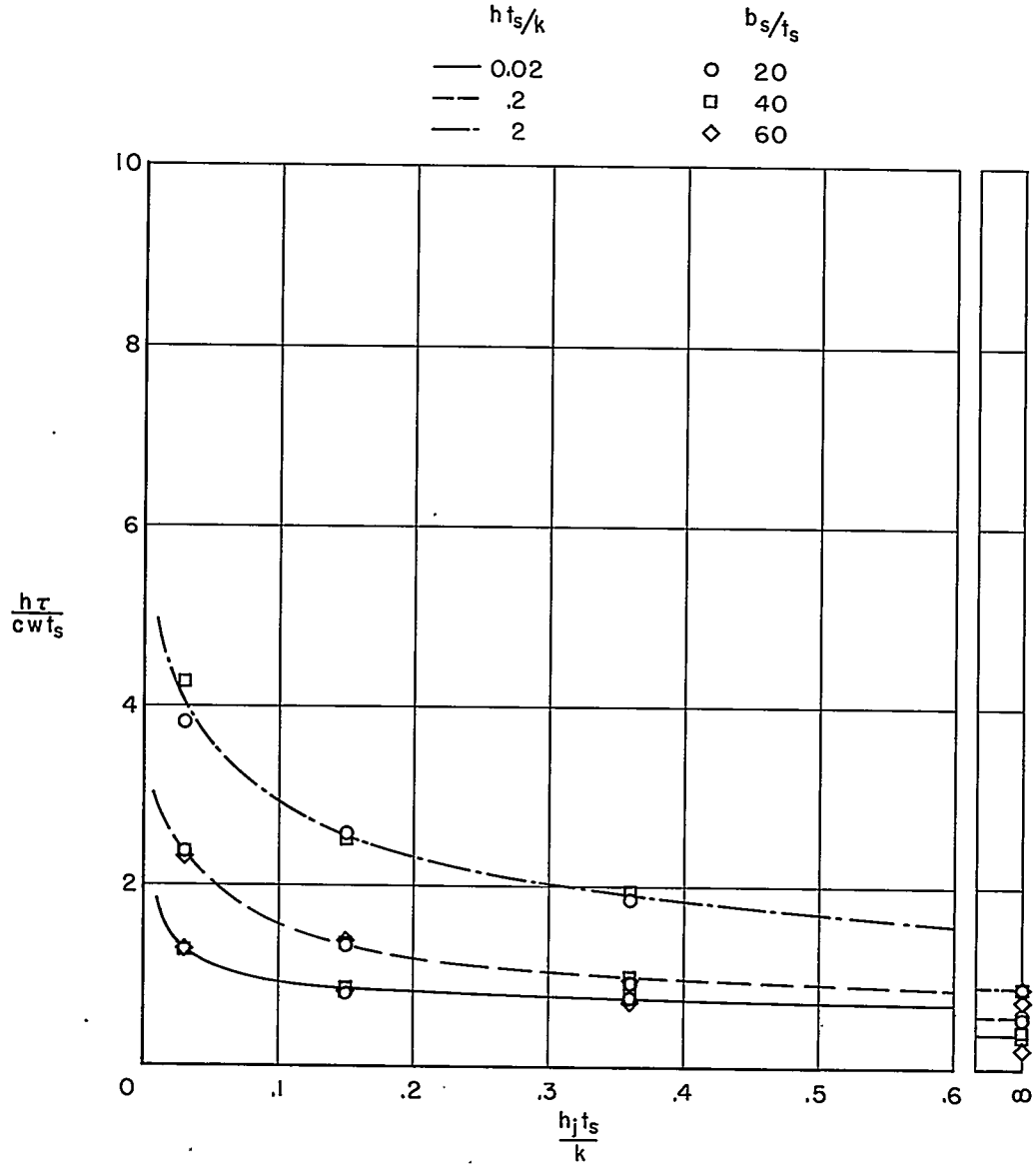

(b) Time parameter.

Figure 16.- Concluded.

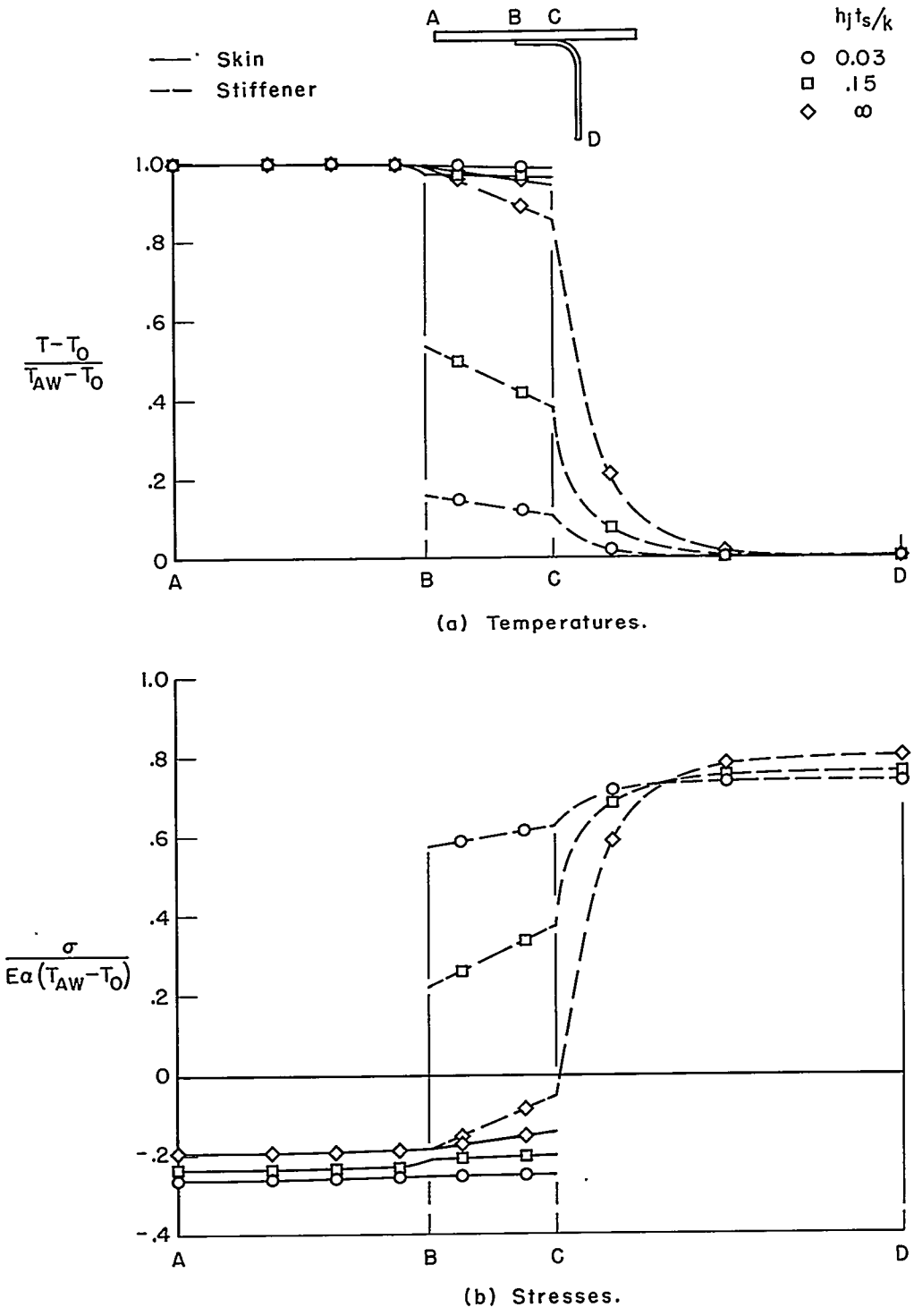

Figure 17.- Distribution of temperature and stress ratios for $ht_s/k = 2$ and $b_s/t_s = 20$.